EurJIC
European Journal of Inorganic Chemistry

Research Article
doi.org/10.1002/ejic.202100898

Chemistry Europe
European Chemical Societies Publishing

www.eurjic.org

# Asymmetrically Difunctionalized 1,1′-Ferrocenyl Metalloligands and Their Transition Metal Complexes

Hanna E. Wagner,[a] Nils Frank,[b] Elham Barani,[b] Christopher E. Anson,[a] Lea Bayer,[a] Annie K. Powell,[a] Karin Fink,[b] and Frank Breher*[a]

*Dedicated to Prof. Dieter Fenske on the occasion of his 80th birthday.*

The synthesis and full characterization of novel 1,1′-difunctionalized ferrocene metalloligands is described. While one cyclopentadienyl ring has been functionalized with 2,2′-bipyridine for secondary coordination, the second Cp ring has been decorated with different aryl moieties containing electron withdrawing groups such as 4-$(CF_3)C_6H_4$ (**2A**) 3,5-$(CF_3)_2C_6H_3$ (**2B**) or 4-$(NO_2)C_6H_4$ (**2C**). The newly developed metalloligands were reacted with $[Pd(cod)Cl_2]$ (**3A**–**C**), $CuCl_2$ (**4A**–**C**) and *trans*-$[(PPh_3)_2Ni(Mes)Br]$ (**5A**,**B**) to obtain the corresponding square-planar and dimeric square-pyramidal complexes. The electrochemical behaviour of the ligands and complexes was investigated with the aid of cyclic voltammetry and compared with the corresponding monofunctionalized derivatives. The influence of the implemented functional groups on the nickel complexes was then confirmed for the reductive elimination reaction of an aryl ether induced by oxidation of the corresponding methoxides (**6A**,**B**,**D**). The experimental findings are supported by quantum chemical calculations.

## Introduction

In recent years, the development of stimuli-responsive ligands, and investigations of their transition metal complexes, has been of major interest for a number of research groups.[1] Ideally reversible changes of the ligating properties of the ligand can be induced by external stimuli such as irradiation with visible light, protonation or redox-switching.[2] Inspired by the pioneering work of Wrighton and co-workers on cobaltocene-based redox-switchable catalysts,[3] many other redox-active ligands and (catalytically active) multimetallic complexes have been developed, the majority of which are based on ferrocenyl (Fc)-containing mono- or multidentate ligands.[4,5] In this context, Fc-decorated phosphines, *N*-heterocyclic carbenes (NHCs) and mesoionic carbenes (MICs) have been investigated. Selected examples are summarised in Scheme 1.

One common feature of ferrocene-based ligands is that in most cases the cyclopentadienyl (Cp) rings of the ferrocenyl entities are either monofunctionalized on one ring or symmetrically difunctionalized at both Cp rings.[4] Even though derivatives possessing a donor group on only one of the Cp rings are predestinated for further functionalization on the other Cp ring (1,1′-difunctionalization), almost no examples are known in the literature where such systems have been targeted for investigation in the area of redox-switchable catalysis. In the case of the presence of additional functional groups on the Cp entities,

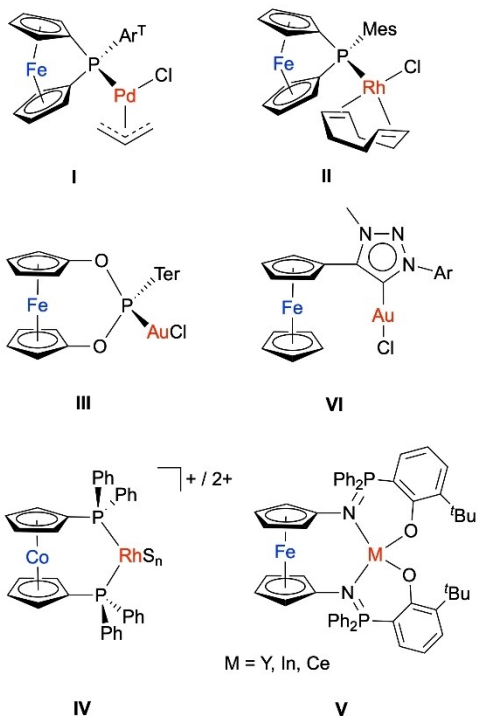


**Scheme 1.** Selected redox-switchable catalysts from the literature.

[a] *Dr. H. E. Wagner, Dr. C. E. Anson, L. Bayer, Prof. Dr. A. K. Powell, Prof. Dr. F. Breher*
*Karlsruhe Institute of Technology (KIT)*
*Institute of Inorganic Chemistry*
*Engesserstraße 15, 76131 Karlsruhe, Germany*
*E-mail: breher@kit.edu*
https://www.aoc.kit.edu/breher/index.php
[b] *N. Frank, E. Barani, Prof. Dr. K. Fink*
*Karlsruhe Institute of Technology (KIT)*
*Institute of Nanotechnology*
*Postfach 3630, 76021 Karlsruhe, Germany*

*Supporting information for this article is available on the WWW under https://doi.org/10.1002/ejic.202100898*

*Part of the "Ferrocene Chemistry" Special Collection.*

Research Article
doi.org/10.1002/ejic.202100898


further tuning of the catalytic system might be possible. The reason why only few examples of asymmetrically 1,1′-difunctionalized ferrocene derivatives are described in literature[6] might result from the lack of suitable synthetic approaches in addition to side reactions, sensitivity of functional groups and low yields.[7]

Herein we report a simple synthetic approach to obtain asymmetrically 1,1′-difunctionalized ferrocene derivatives by implementing additional functional groups. The effect of the additional groups is studied on a set of transition metal complexes using cyclic voltammetry. The experimental findings are supported by density functional theory (DFT) calculations.

## Results and Discussion

### Synthesis and Characterization

The key to the described synthetic approach to obtaining asymmetric derivatives is the stepwise functionalization of a symmetrically difunctionalized ferrocene. A conceivable synthetic route for a suitable starting material involves a symmetric difunctionalization of ferrocene *via* lithiation and subsequent conversion in order to obtain functional groups such as e.g. stannanes or boronic acid entities, which are suitable for cross-coupling reactions at both Cp-rings. Due to their lower toxicity and simplified purification methods, boronic acid derivatives were selected. The straightforward synthesis is outlined in Scheme 2.[7b,8]

The thus obtained 1,1′-ferrocene diboronic acid has previously been applied for asymmetric functionalization *via* cross-coupling reactions, but until now few examples have been described.[9] A significant disadvantage of the diboronic acid is its tendency to form aggregates due to intermolecular hydrogen bonds.[6b] In the scope of this work, these aggregates led to an impairment of the subsequent postfunctionalization. We found that this problem can be circumvented by using the corresponding pinacol ester. This pinacol ester is well-established in the synthesis of symmetric 1,1′-ferrocenyl derivatives,[9] but despite the obvious advantages it has never been used for the synthesis of asymmetrically functionalized compounds.

The synthesis of the pinacol ester starting from ferrocene was carried out according to literature procedures (Scheme 2).[10] For the first functionalization at the 1-position, $Fc(Bpin)_2$ was reacted in a Suzuki-Miyaura coupling reaction with 5-bromo-2,2′-bipyridine.[11] The reaction conditions for the coupling reaction are based on similar reactions described in the literature (Scheme 2).[6,12] Compound **1** crystallizes in the monoclinic space group $P2_1/n$ and the molecular structure is shown in Figure 1. The spatial demands of the pinacol ester unit leads to a torsion of both functional groups of with an angle of about 113° and a staggered arrangement of both Cp rings. A clear advantage of **1** with regard to a second functionalization is its stability towards air and moisture and thus large quantities can easily be stored.

The second functionalization can be performed in an analogous manner to the first (Scheme 3). In the present work, we focused on electron-withdrawing groups in order to investigate their electronic effects on both the ferrocenyl entity itself and the subsequently *N*,*N*′-coordinated metal atom. The advantage of this two-step functionalization is that the second reagent, especially when liquid, can be used in excess and is easy to remove. For ligands **2A** and **2B**, the procedure results in (very) high yields of 75–92%. Ligand **2C** was obtained in 56% isolated yield.

All three ligands are obtained as red (**2A**, **2B**) to dark red (**2C**) powders that are not sensitive to air and moisture. The

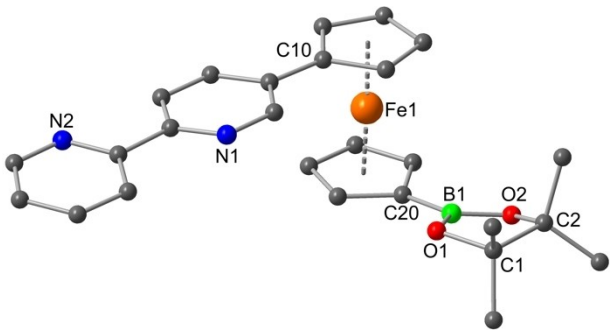


**Figure 1.** Molecular structure of **1**. Hydrogen atoms have been omitted for clarity. Selected bond lengths [pm] and angles [°]: C10–C31 146.5(2), C20–B1 154.1(3), τ = 97.17°, torsion angle Cp-bipy 2.02° (τ = angle between the substituents along the ferrocene axis, *i.e.* Bpin and bipy).

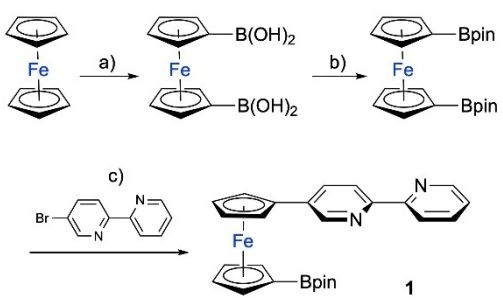


**Scheme 2.** Synthesis of 1,1′-Fc(bipy)(Bpin) (**1**). Reaction conditions: a) 1. *n*-BuLi, TMEDA, 2. $(n\text{-BuO})_3B$, 3. KOH, $H_2SO_4$; b) pinacole; c) $[Pd(dppf)Cl_2]$, NaOH, $Na_2CO_3$, DME, 1,4-dioxane.

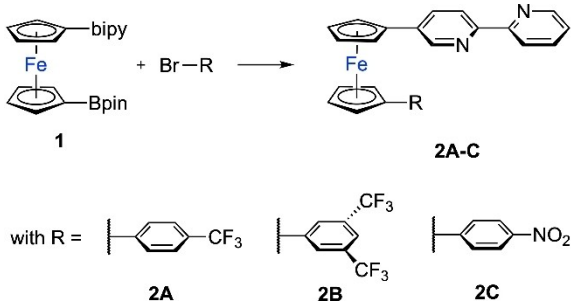


**Scheme 3.** Synthesis of the ligands **2A**, **2B** and **2C** via Suzuki-Miyaura cross-coupling. Reaction conditions: $[Pd(dppf)Cl_2]$, NaOH, $Na_2CO_3$, DME, 1,4-dioxane.

Research Article
doi.org/10.1002/ejic.202100898



NMR spectroscopic investigations in $CD_2Cl_2$ already reveal very similar spectra and thus very similar structures. The chemical shifts of the protons of the ferrocene backbone ($\delta^{1H}$ = 4.3–4.8 ppm) and the bipyridyl entity ($\delta^{1H}$ = 7.1–8.7 ppm) are in the same region as the ones of the monofuntionalized 5-ferrocenyl-2,2′-bipyridine, which were first described by Crowley.[12]

Figure 2 shows the molecular structures of the ligands **2A** and **2C**. In case of compound **2B**, only small crystals could be obtained where crystal structure analysis confirmed the connectivity, but the data set was of poor quality. The bond lengths and angles prove similarities to the monofuntionalized 5-ferrocenyl-2,2′-bipyridine ligands of Crowley.[12] The molecular structures of the ligands are essentially unaffected by the additional organic substituent on the second Cp ring.

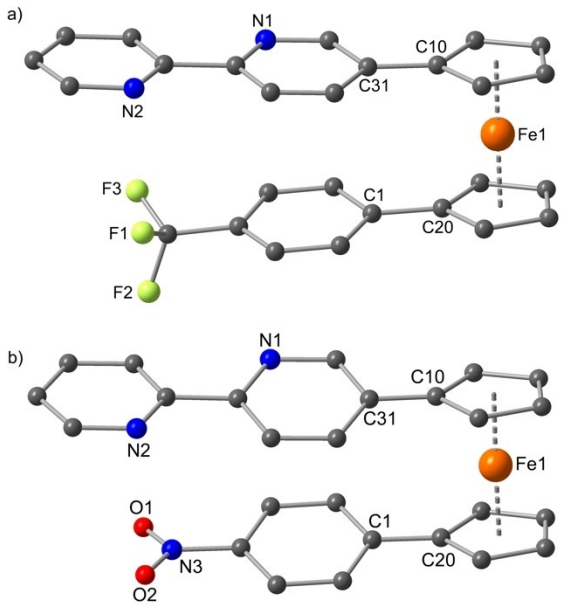


**Figure 2.** Molecular structures of **2A** (a) and **2C** (b). Hydrogen atoms have been omitted for clarity. Selected bond lengths [pm] and angles [°]: a) C10–C31 145.1(8), C20–C1 146.2(9), τ = 0.51°, torsion angle Cp-bipy 4.34°, torsion angle Cp-phenyl 7.21°. b) C10–C31 147.4(3), C20–C1 147.1(3), τ = 2.68°, torsion angle Cp-bipy 17.07°, torsion angle Cp-phenyl 19.11° (τ = angle between the substituents along the ferrocene axis, *i.e.* R and bipy).

For these two compounds, the ferrocene backbones show an ecliptic arrangement. The two aryl substituents adopt a stacked (*syn*) conformation and are parallel to each other, which is likely the result of by π-stacking.[13] Similar effects have been observed by Crowley and co-workers.[6e,f] We note in passing that in solution the proton signals associated with the bipyridyl rings of **2A**–**2C** are slightly shifted upfield relative to those of the singly functionalized compound **2D**,[12] indicating that the di-functionalized ferrocene derivatives might also adopt a stacked (*syn*) conformation in solution (Figure S26, Supporting Information).[6e,f] However, $^1H,^1H$ NOESY and $^1H,^{19}F$ HOESY measurements on **2A** as representative of the newly synthesized ligands gave no indications for π interactions in solution. The comparison with other compounds known from the literature shows that the bond lengths and angles are similar.[14] The bipyridine unit resembles other 2,2′-bipyridine derivatives, which was already shown for the analogous monofunctionalized 5-ferrocenyl-2,2′-bipyridine ligands[12] and it thus seems reasonable to assume that the coordination behavior is similar. To verify this, the ligands were reacted with different transition metal precursors of group 8 and 10. For reference to the electrochemical investigations planned on the free pro-ligands and all their complexes, the complexes of the monofunctionalized 5-ferrocenyl-2,2′-bipyridine of the Crowley group were also synthesized.[12] In the current paper we denote this literature-known ligand as **2D** in the following discussion.

We thus first reacted the pro-ligands **2A**–**2D** with [Pd(cod)$Cl_2$] in order to obtain the square-planar Pd(II) complexes (Scheme 4). For the sake of completeness and subsequent electrochemical comparison, the literature-known complex **3D**[12] with ligand **2D** was also synthesized. As copper(II)

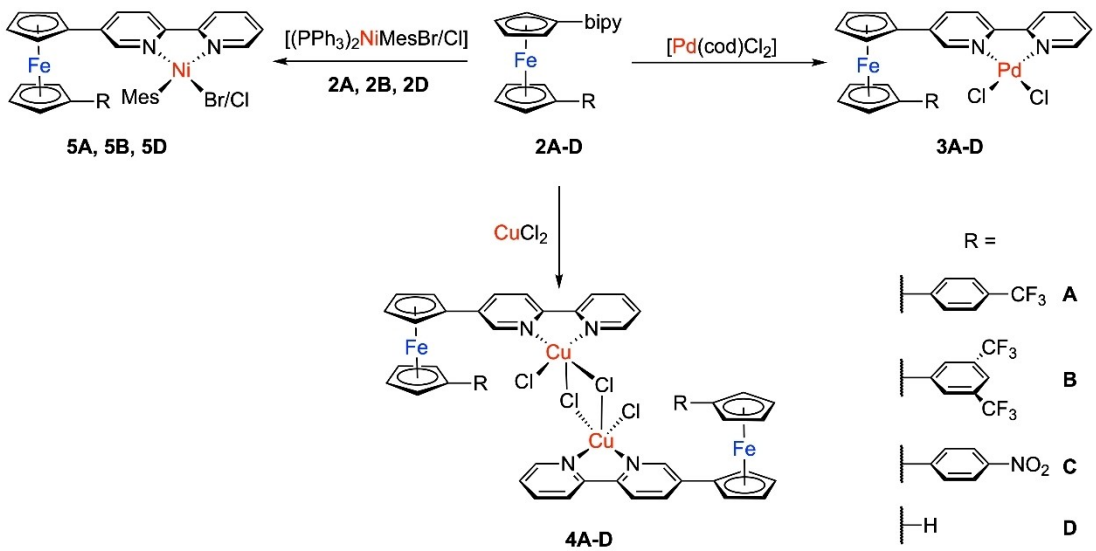


**Scheme 4.** Synthesis of the Pd, Cu and Ni complexes of the metalloligands **2A**–**D**.

Research Article
doi.org/10.1002/ejic.202100898



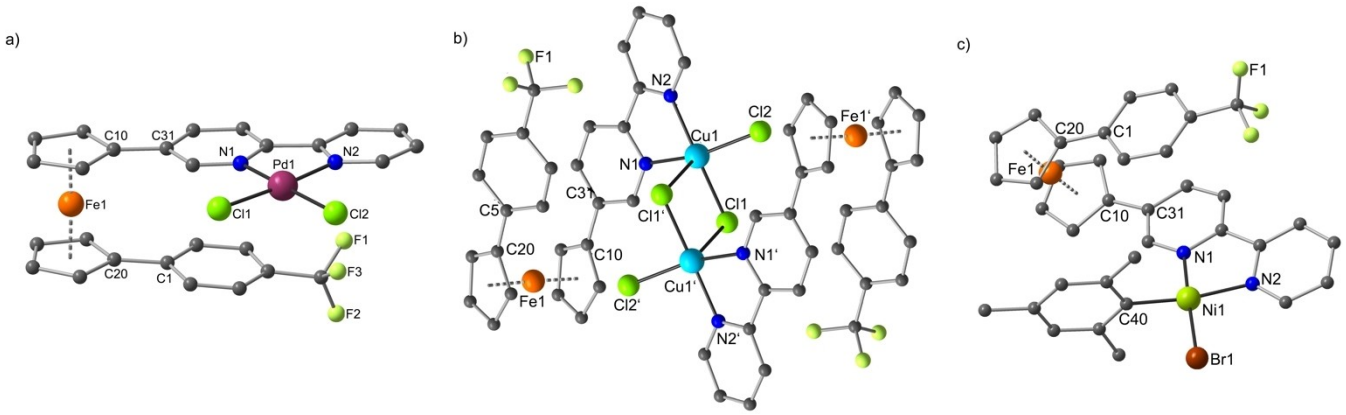


**Figure 3.** Molecular structures of **3A** (a), **4A** (b) and **5A** (c). Hydrogen atoms, any lattice solvent molecules and minor disorder components have been omitted for clarity, for **3A** only the first of the two molecules in the asymmetric unit is shown. Selected bond lengths [pm] and angles [°],[values of the second molecule in the asymmetric unit]: a) C10–C31 145.8(7) [146.2(8)], C20–C1 146.8(8) [147.1(9)], Pd1–N1 204.0(4) [202.1(4)], Pd1–N2 201.7(4) [202.3(4)], Pd1–Cl1 227.84(16) [228.56(15)], Pd1–Cl2 227.93(16) [228.29(16)], N1–Pd1–N2 80.94(17) [80.68(18)], Cl1–Pd1–Cl2 89.75(6) [89.34(6)], N1–Pd1–Cl1 95.04(12) [94.54(13)], N2–Pd1–Cl2 94.36(2) [95.40(13)], N1–Pd1–Cl2 174.25(13) [175.86(13)], N2–Pd1–Cl1 175.65(12) [174.93(13)], $\tau = 2.97°$ [9.21°]; b) C10–C31 145.9(3), C20–C1 147.0(3), Cu1–N1 203.42(19), Cu1–N2 203.17(18), Cu1–Cl1 230.44(9), Cu1–Cl2 226.00(10), Cu1–Cl1′ 267.31(9), N1–Cu1–N2 79.59(7), Cl1–Cu1–Cl2 92.00(4), N1–Cu1–Cl1 94.05(6), N2–Cu1–Cl2 91.43(6), N1–Cu1–Cl2 160.86(5), N2–Cu1–Cl1 169.21(5), Cl1–Cu1–Cl1′ 87.13 (2), Cl2–Cu1–Cl1′ 101.41(3), N1–Cu1–Cl1′ 97.02(5), N2–Cu1–Cl1′ 102.20(6), $\tau = 0°$; c) C10–C31 147.1(3), Ni1–N1 190.83(19), Ni1–N2 198.0(2), Ni1–Br1 227.59(7), Ni1–C40 190.1(2), N1–Ni1–N2 82.56(8), Br1–Ni1–C40 89.37(7), N1–Ni1–C40 92.63(9), N2–Ni1–Br1 96.13(6), N1–Ni1–Br1 173.94(6), N2–Ni1–C40 171.40(9), $\tau = 1.92°$ ($\tau$ = angle between the substituents along the ferrocene axis, *i.e.* R and bipy).

complexes of bipyridine ligands are well-known for their interesting coordination behaviour,[15] the ligands in this work were also reacted with $CuCl_2$. The resulting dimeric complexes **4A**–**D** consist of two metalloligand entities coordinating two copper atoms in square-pyramidal coordination environments and a chlorine atom serving as a bridging atom. Lastly, the synthesized ligands were reacted with a nickel precursor $[(PPh_3)_2Ni(Mes)Br/Cl]$ containing a mesityl group. This was motivated by the idea that similar square-planar compounds containing aryl and alkoxide groups show reductive elimination reactions when the nickel is oxidized. Therefore, the nickel compounds **5A**, **5B** and **5D** were synthesized according to the method of Klein.[16] All performed complexation reactions are summarized in Scheme 4.

Only small crystals could be obtained for almost all synthesized complexes. Here the chemical connectivity could be proved with the help of the SCXRD measurements. For the reaction of 5-ferrocenyl-2,2′-bipyridine with $CuCl_2$, a sparingly soluble orange solid was obtained. All efforts to obtain larger crystals failed. Nevertheless, the chemical composition is analogous to the other copper complexes, which was supported using elemental analysis. As not all crystal data sets comply with the requirements for publication, Figure 3 exemplifies the molecular structures of all complexes obtained with ligand **2A**.

The molecular structures of the complexes show the expected coordination pattern of all three transition metal precursors. All bond lengths and angles such as *d*(Pd–N) ≈ 204 pm, *d*(Cu–N) ≈ 203 pm, *d*(Ni–N) ≈ 190–198 pm are in very good agreement with similar bipyridine complexes containing the metals used in this study. No structural influence of the different functional groups could be observed. This fact confirms our approach of adding auxiliary functional groups to serve as fine tuning tools for optimization of redox-switchable metalloligands within the context of the fundamental idea. The staggered arrangement of the aryl substituents caused by π-stacking for compounds **3A** and **4A** still remains. The steric bulk of the mesityl entity of complex **5A** hinders this arrangement leading to a small distortion of the aryl rings. The structural motif of the copper complex **4A** is typical for $CuCl_2$-containing bipyridine complexes with numerous examples of similar compounds described in the literature.[15]

In the case of the nickel complexes, $^1$H NMR spectroscopic data show an equilibrium between the *SP*-4-3 and *SP*-4-2 isomers (Scheme 5), whereas the molecular structure in Figure 3 only shows the *SP*-4-2 isomer.

As a result of the synthetic protocol used and the associated purification method to synthesize the nickel precursor $[(PPh_3)_2Ni(Mes)Br/Cl]$, the latter contains small amounts of a chloride instead of bromide ligand leading to additional signals in the corresponding NMR spectra (Figure 4). Since this kind of impurity, as well as the *SP*-4-3⇌*SP*-4-2 equilibrium, have no effects in terms of this part of the work no further attention has been paid to the study of their disaggregation. In the crystal used for the structure determination, apparently only bromide was present.

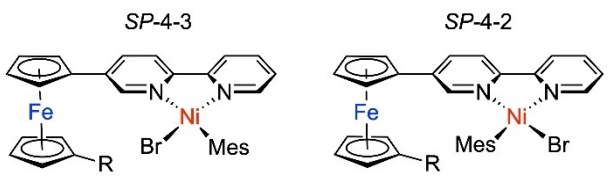


**Scheme 5.** Configuration indexes for both isomers in **5A**, **5B**, **5D**.

Research Article
doi.org/10.1002/ejic.202100898



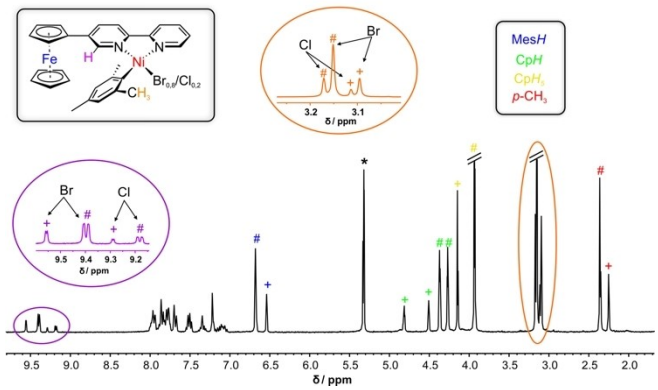


**Figure 4.** $^1$H NMR spectrum of compound **5D** in $CD_2Cl_2$. Signals are denoted as follows: + = *SP*-4-3 isomers, # = *SP*-4-2 isomers (* = $CDHCl_2$).

## Cyclic Voltammetry Studies

All compounds under study were investigated with the aid of cyclic voltammetry.[5,17] Firstly, the pro-ligands were investigated. The newly synthesized 1,1′-difunctionalized ligands **2A**–**2C** of this work were compared with Crowley's monofunctionalized 5-ferrocenyl-2,2′-bipyridine **2D**. Nitrosyl functional groups as present in ligand **2C** usually exhibit a more complex electrochemical behavior compared with $CF_3$-groups making a direct comparison difficult.[18] Additionally, during our measurements, electrochemical interactions of nitrosyl-containing compounds with the employed internal reference were observed.

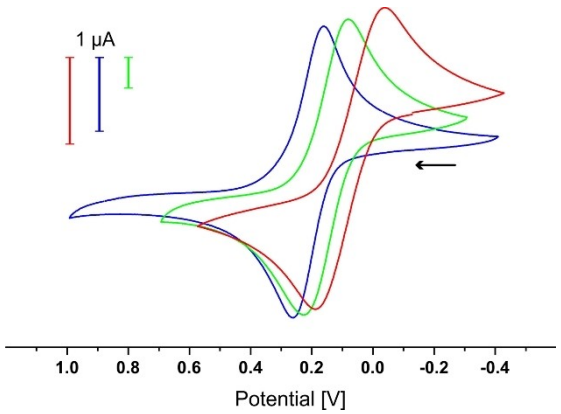


**Figure 5.** Cyclic voltammograms of **2D** (red) **2A** (green) and **2B** (blue) in $CH_2Cl_2$. All measurements at room temperature vs. the $Fc/Fc^+$ couple; scan rate $v = 250$ mV s$^{-1}$, Pt/[$^n$Bu$_4$N][PF$_6$]/Ag.

Thus, the discussion of the electrochemical data is limited to ligands **2A**, **2B** and **2D** (Figure 5). As expected, the half-wave potential of the Fc-based redox-couple is anodically shifted with an increasing number of $CF_3$-groups. $E^0_{1/2}$ for ligand **2A** was found to be 154 mV (*vs.* $Fc/Fc^+$) and therefore ca. 80 mV more positive than the potential of the monofunctionalized derivative ($E^0_{1/2}$(**2D**) = 77 mV). The potential of ligand **2B** ($E^0_{1/2}$ = 211 mV) is further shifted by + 60 mV as compared to ligand **2A** (Table 1).

The observed substituent-dependent trends were also observed for the corresponding complexes. Table 1 summarizes the half-wave potentials for the Fc-based redox couple of all investigated compounds. The shift of the redox potentials depends on both the coordinated metal fragments and the attached functional groups. For example, the palladium and copper complexes show ca. + 100 mV more positive redox potentials than those for the pro-ligands. By contrast, the $E^0_{1/2}$ values of the nickel complexes **5A**, **5B**, and **5D** are almost unaffected with regard to the corresponding free ligands. It appears that both influences, *i.e.* the one exerted by the coordination of the metal fragment and the one of the electron-withdrawing groups, are in balance. Further cyclic voltammograms for all compounds are given in the Supporting Information.

In order to gain insights into the influence of the attached functional groups on the *N*,*N*′-coordinated metal fragments, the nickel complexes were subjected to further investigations. As nickel complexes containing aryl and alkoxide groups are well-known for undergoing reductive elimination reactions after oxidation of the nickel atom from Ni(II) to Ni(III), the analogue methoxides **6A**, **6B**, and **6D** were synthesized by salt metathesis from **5A**, **5B**, and **5D** using NaOMe (Scheme 6).[19] MacMillan and co-workers used similar compounds in their work on nickel-catalyzed cross-coupling reactions to investigate the reductive elimination step with the help of cyclic voltammetry.[19b] Inspired by this work, we aimed to influence and optimize catalytic activities, such as reductive eliminations, by fine-tuning the ligands using various additional functional groups.

The formation of the corresponding and highly sensitive methoxides was confirmed by NMR spectroscopy. The cyclic voltammograms of the resulting products are shown in Figure 6. In this case, the redox potentials depend strongly on the attached functional groups. Beside the quasi-reversible redox wave belonging to the Fc-based Fe(II)/Fe(III) redox couple, further irreversible oxidation is observed at ca. $E_{pa}$(**6D**) = −100 mV, $E_{pa}$(**6A**) = −50 mV and $E_{pa}$(**6B**) = + 100 mV, which can be related to the oxidation of the nickel atom, and subsequent reductive elimination of Mes–OMe.

**Table 1.** Half-wave potentials of the compounds in $CH_2Cl_2$ at room temperature (vs. $Fc/Fc^+$).[a]

| | $E^0_{1/2}$ [mV] | | $E^0_{1/2}$ [mV] | | $E^0_{1/2}$ [mV] | | $E^0_{1/2}$ [mV] |
|---|---|---|---|---|---|---|---|
| **2D** | 77 | **3D** | 175 | **4D** | 168 | **5D** | 53 |
| **2A** | 154 | **3A** | 260 | **4A** | 255 | **5A** | 159 |
| **2B** | 211 | **3B** | 314 | **4B** | 319 | **5B** | 257 |

[a] scan rate $v = 100$ mV s$^{-1}$, Pt/[$^n$Bu$_4$N][PF$_6$]/Ag.

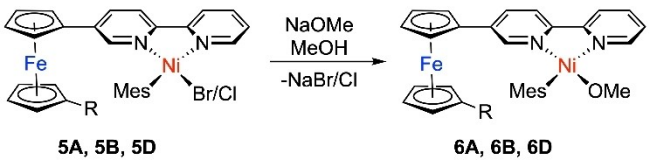


**5A, 5B, 5D** **6A, 6B, 6D**

**Scheme 6.** Synthesis of the methoxides **6A**, **6B** and **6D**.

Research Article
doi.org/10.1002/ejic.202100898


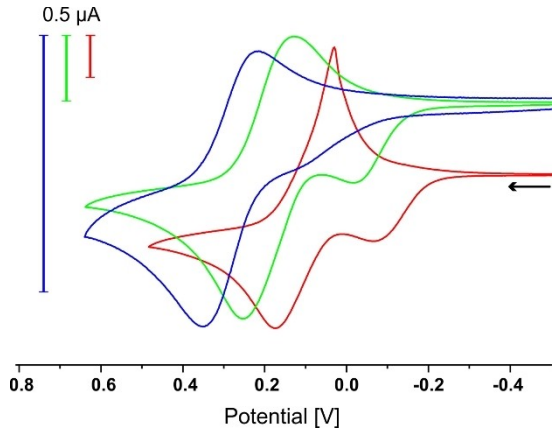


**Figure 6.** Cyclic voltammograms of **6D** (red), **6 A** (green) and **6B** (blue) in $CH_2Cl_2$. All measurements at room temperature vs. the $Fc/Fc^+$ couple; scan rate $v = 100\ mV\,s^{-1}$, Pt/[$^nBu_4N$][$PF_6$]/Ag.

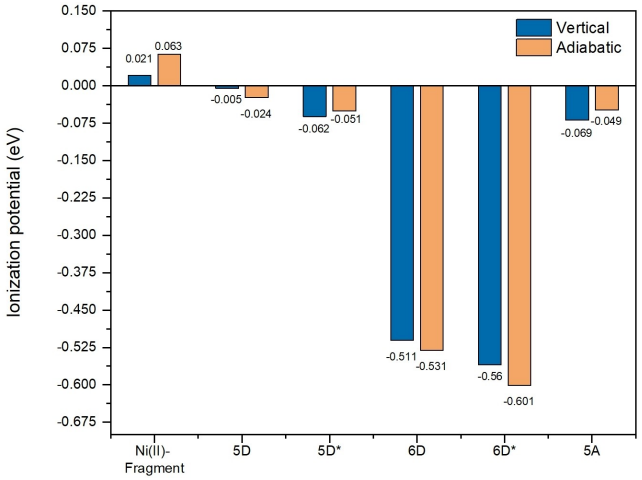


**Figure 7.** Ionization potential (B3LYP) with respect to the calculated values for ferrocene (6.363 eV vertical and 6.228 eV adiabatic, respectively, see Table S3 of the Supporting Information).

The anodic shift of the irreversible oxidation caused by the electron withdrawing groups can also be observed, implying a significant contribution from the attached functional groups on both to the ferrocene and bipyridine entities. From this a potentially catalytically active metal fragment is implied. In other words, the difunctionalization of the ferrocene backbone with additional groups results in it exerting an electronic influence on the secondary coordinated metal center.

Inspired by MacMillan's nickel-catalyzed cross-coupling reactions,[19b] the complexes **6A**, **6B**, and **6D** were used to study a potential bimetallic cooperative catalysis.[2a] Firstly, the reductive elimination was confirmed by chemical oxidation of the compounds on a preparative scale, monitored using GC-MS measurements where the formation of the generated aryl ether 2,4,6-trimethylanisole was verified. However, under the conditions used for a catalytic system (12 h, rt), no turnover could be observed.

## Quantum Chemical Calculations

To further support the electrochemical findings and to find an explanation of the inactivity of the bimetallic complexes in catalytic cross-coupling, quantum chemical calculations were performed on **5A**, **5D**, and **6D**. Initially, we aimed to obtain information about the differences in the ionization potential of Ni(II) and Fe(II). To this end, the gas phase ionization potentials (IP) of **5D** and **6D** were calculated and the site of ionization within the molecule was located. The results were compared to calculations on model systems **5D*** and **6D***. In these model systems, Fe was substituted by an all electron pseudopotential (see Experimental Section) so that ionization could only take place at Ni. For further comparison, a Ni fragment of **5D** where ferrocenyl was substituted by hydrogen was used and all ionization potentials were compared to ferrocene. The results are summarized in Figure 7.

The calculated ionization potentials of **5D** and **5A** were very similar and close to the value of ferrocene. Only slightly more negative values were found for **5A** (−0.069 eV vertical; −0.049 eV adiabatic) as compared to **5D** (−0.005 eV vertical; −0.024 eV adiabatic), which show the same tendency although much less pronounced as expected from the electrochemical findings in solution ($\Delta E^0_{1/2}$(**5A**/**5D**) = 106 mV). The same holds for a Ni(II) fragment of the complex. Interestingly, according to the spin density (see Figure S4), ionization takes mainly place at Ni(II). Similar trends have already been observed by us for related complexes of ferrocenyl-functionalized *N*-donor ligands.[5e] For hybrid functionals, the spin density is completely localized on Ni. In the case of GGA (general gradient approximation) functionals, there is a significant contribution on Fe. In **6D**, the ionization is favored by about 0.5 eV compared to ferrocene and the spin density shows contributions on the oxygen of OMe. These results are supported by quasi particle energies obtained by GW calculations (see Experimental Section), which allow to differentiate between the lowest ionization from a Ni and a Fe orbital (See Table 2 and Tables S3–S6). Although they were treated by a slightly different basis set (for details, see the Supporting Information), the IPs of the model complexes **5D*** and **6D*** were similar to the results for **5D** and **6D** indicating that they are appropriate for the investigation of the transition states and barriers for the reductive elimination and the oxidative addition. A second limitation of the model is that solvent effects are neglected, which can stabilize various species to different extents. The following combinations of oxidation states were probed: Ni(II)/Fe(II) and Ni(II)/Fe(III) (cf. Figure 8) as well as Ni(III)/Fe(II) and Ni(III)/Fe(II) with additional $Br^-$ coordinating the Ni site (cf. Figure 9). Several conclusions can be drawn from the reaction profiles depicted in Figure 8 and Figure 9:

The reductive elimination seems only feasible on a Ni(III) center, as already shown in the literature.[19b] Nevertheless, the envisioned bimetallic cooperative catalysis through the electrostatically modelled ferrocenyl-unit does not significantly lower

Research Article
doi.org/10.1002/ejic.202100898



**Table 2.** Comparison of the vertical ionization potential and quasi particle energies of the highest Ni and Fe dominated orbital, respectively, for **5D** (**5A** for comparison) and **6D** (def2-TZVP basis set). The Mulliken populations refer to the Ni and Fe contributions in the respective orbitals. More details are given in the Supporting Information, Tables S3–S6 and Figure S4.

| Model system | Functional | Vertical ionization potential [eV] | Ni/Fe (Mulliken population) | Ni/Fe (orbital energy [eV]) | Ni/Fe (quasiparticle energy [eV]) |
|---|---|---|---|---|---|
| **5D** | B3LYP | 6.358 | 0.8/0.8 | 5.530/5.714 | 6.420/6.234 |
| | PBE0 | 6.269 | 0.7/0.8 | 5.956/6.256 | 6.498/6.341 |
| | TPSS | 6.208 | 0.9/0.6 | 4.315/4.675 | 6.541/6.412 |
| | TPSSH | 6.358 | 0.9/0.7 | 4.935/5.245 | 6.401/6.364 |
| **5A** | B3LYP | 6.294 | 0.8/0.8 | 5.589/5.917 | 6.477/6.367 |
| | PBE0 | 6.310 | 0.7/0.8 | 5.998/6.415 | 6.560/6.502 |
| **6D** | B3LYP | 5.852 | 0.4/0.8 | 4.802/5.616 | 5.997/6.140 |
| | PBE0 | 5.951 | 0.4/0.6 | 5.162/6.153 | 6.084/6.596 |
| | TPSS | 5.744 | 0.5/0.4 | 3.907/4.525 | 5.982/6.376 |
| | TPSSH | 5.845 | 0.5/0.7 | 4.373/5.118 | 5.928/6.258 |

the activation barrier (Figure 8), at least for this catalytic model system.[5a]

In contrast to what is the existing literature,[20] our investigations show that an oxidative addition on a Ni(I) center is kinetically as well as thermodynamically achievable. This finding could motivate the development of cross-coupling cycles relying solely on the Ni(III)/Ni(I) redox couple.

Furthermore, the additional coordination of a solution state $Br^-$ anion to the nickel unit raises the activation energies of the reductive elimination and oxidative addition dramatically (Figure 9). This self-poisoning of the active catalytic site gives a possible explanation as to why only stoichiometric and no catalytic turnover was observed experimentally. This result could stimulate the use of moderately coordinating pseudo-halides, like aryl triflates, as coupling partners.[21]

Additionally, highly exergonic binding of the substrate Mes–Br and product Mes–OMe to a low-coordinate Ni atom could be interpreted as thermodynamic resting states limiting the turnover frequency.

## Conclusion

In summary, we have introduced a simplified synthetic procedure to obtain 1,1′-difunctionalized ferrocene derivatives with very high yields and the prospect of a wide variety of different substituents. This procedure opens new directions concerning individual fine-tuning of redox-active ligand systems. Furthermore, the investigations of this new synthetic strategy are complemented by several coordination compounds resulting from the new pro-ligands and different palladium, copper and nickel precursors. Finally, the electrochemical properties of the compounds under study were investigated and thoroughly compared with each other in order to scrutinize the slight but remarkable differences caused by the implementation of different electron withdrawing groups. The influence of the latter on the nickel complexes was subsequently confirmed for the reductive elimination reaction of an aryl ether induced by oxidation of the corresponding methoxides. Quantum-chemical calculations unravel details about the reductive elimination and oxidative addition taking place at the Ni site and show the strong dependence on both the oxidation state and the coordination sphere of the metal. Several possible reasons were identified to help understand why the experimentally observed reductive elimination could not be translated into a bimetallic catalytic system.

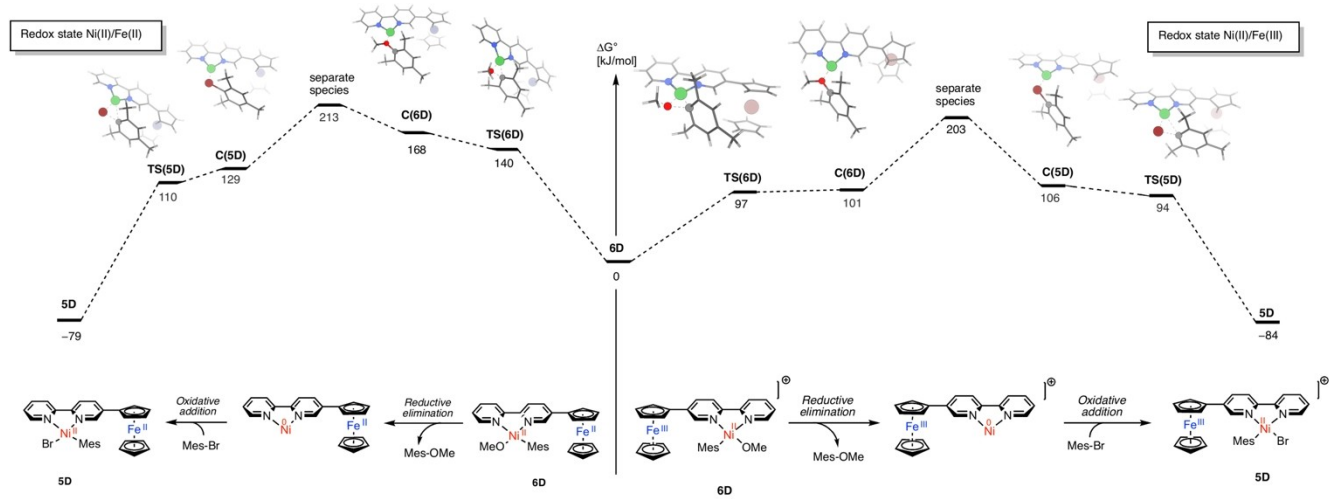


**Figure 8.** Gibbs free energy profile for a catalyst in oxidation states Ni(II)/Fe(II) and Ni(II)/Fe(III). All potentials include the energy of Mes–OMe and Mes–Br (one interacting with the catalyst, the other one infinitely separated) in order to limit changes in the interaction energy between substrate and catalyst (See Table S2 of the Supporting Information). Separate species means that Mes–OMe and Mes–Br are both at infinite distance.

Research Article
doi.org/10.1002/ejic.202100898



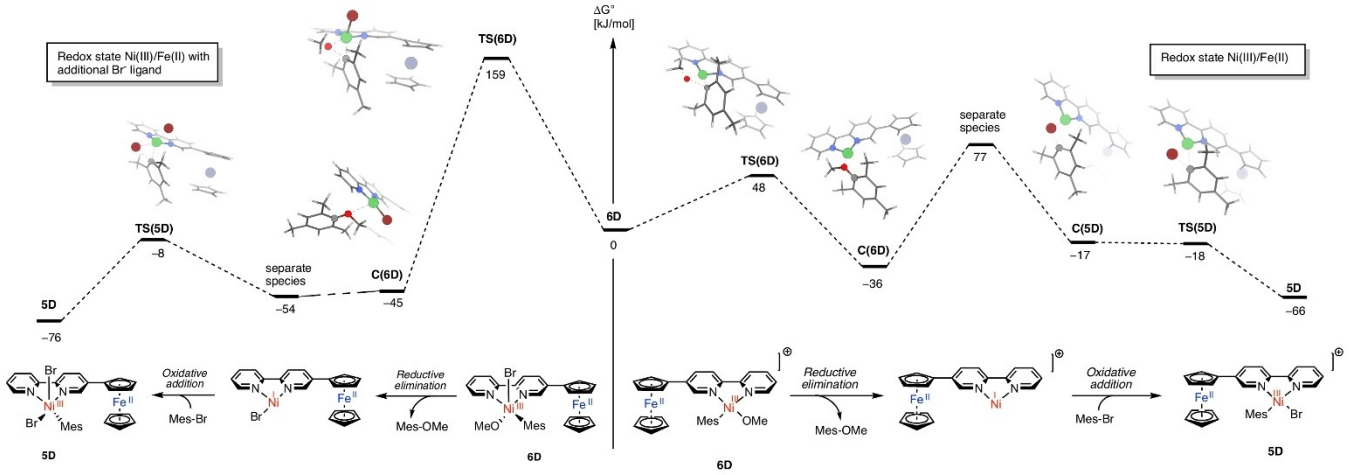


**Figure 9.** Gibbs free energy profile for a catalyst in oxidation states Ni(III)/Fe(II) with and without an additional $Br^-$ anion coordinating at the Ni site. All potentials include the energy of Mes–OMe and Mes–Br (one interacting with the catalyst, the other one infinitely separated) in order to limit changes in the interaction energy between substrate and catalyst (See Table S2 of the Supporting Information). Separate species means that Mes–OMe and Mes–Br are both at infinite distance.

## Experimental Section

### General methods and materials

All manipulations, except of aqueous work-ups, were carried out with standard Schlenk line techniques. 1,1′-Fc(Bpin)$_2$ has been synthesized according to literature methods[10a,b] and the obtained analytical data were compared with literature values.[10c] Methylene chloride and acetonitrile were freshly distilled in an argon atmosphere from calcium hydride. Toluene, diethyl ether, 1,4-dioxane, DME and tetrahydrofuran were dried using sodium/benzophenone ketyl. $CD_2Cl_2$ was vacuum transferred from calcium hydride while $C_6D_6$ was vacuum transferred from sodium/benzophenone ketyl into thoroughly dried glassware equipped with Young Teflon valves.

$^1$H, $^{11}$B, $^{13}$C and $^{19}$F NMR spectra were recorded with Bruker AV 300 and 400 spectrometers in dry deuterated solvents. The chemical shifts are expressed in parts per millions and $^1$H and $^{13}$C signals are given relative to TMS. $^{11}$B and $^{19}$F are given relative to $BF_3{\cdot}OEt_2$ and $CFCl_3$. Coupling constants J are given in Hertz as positive values regardless of their real individual signs. The multiplicity of the signals is indicated as s, d, q, sept or m for singlets, doublets, quartets, septets or multiplets, respectively. The assignments were confirmed as necessary with the use of 2D NMR correlation experiments. Mass spectrometry measurements were performed on an Advion expression$^L$ CMS mass spectrometer under atomic pressure chemical ionization (APCI) IR spectra were measured with a Bruker Alpha spectrometer using the attenuated total reflection (ATR) technique on powdered samples, and the data are quoted in wavenumbers ($cm^{-1}$). The intensity of the absorption band is indicated as vw (very weak), w (weak), m (medium), s (strong), vs. (very strong) and br (broad). Melting points were measured with a Thermo Fischer melting point apparatus and are not corrected.

Elemental analyses were carried out in the institutional technical laboratories of the Karlsruhe Institute of Technology (KIT).

Cyclic voltammetry measurements were performed with a Metrohm potentiostat (PGSTAT101) and an electrochemical cell within a glovebox. We used a freshly polished Pt disk working electrode, a Pt wire as counter electrode, and a Ag wire as (pseudo) reference electrode ([$n$Bu$_4$N][PF$_6$] (0.1 M) as electrolyte). Potentials were calibrated against the Fc/Fc$^+$ couple (internal standard).

**Synthesis of 1**: 5-Bromo-2,2′-bipyridine (1.50 g, 6.39 mmol), 1,1′-Fc(Bpin)$_2$ (2.80 g, 6.39 mmol) and [Pd(dppf)Cl$_2$] (0.468 g, 0.639 mmol) in a Schlenk flask were dissolved in 45 mL DME and 45 mL 1,4-dioxane. Then, 15 mL of a degassed aqueous solution of $Na_2CO_3$ (1 M) and 5 mL of a degassed aqueous solution of NaOH (3 M) were added and the reaction mixture was heated to 85 °C f 40 h. After cooling to room temperature, the reaction mixture was added on ice and extracted with EtOAc. The organic layer was washed with a saturated aqueous solution of $NH_4Cl$, water and brine and dried over $MgSO_4$. After removing all volatile components the crude product was purified by column chromatography (silica gel cyclohexane: EtOAc (4:1)). The product was isolated as an orange solid. Yield: 2.50 g (84%). Mp. (sealed tube): 169 °C; $^1$H NMR ($C_6D_6$, 300.13 MHz): $\delta = 1.15$ (s, $CH_3$, 12H), 4.02 (dd, $^3J_{HH} = 1.6$ Hz, $^3J_{HH} = 1.6$ Hz, $H_{Cp}$, 2H), 4.25 (dd, $^3J_{HH} = 1.9$ Hz, $^3J_{HH} = 1.9$ Hz, $H_{Cp}$, 2H), 4.44 (dd, $^3J_{HH} = 1.6$ Hz, $^3J_{HH} = 1.6$ Hz, $H_{Cp}$, 2H), 4.50 (dd, $^3J_{HH} = 1.7$ Hz, $^3J_{HH} = 1.7$ Hz, $H_{Cp}$, 2H), 6.72 (ddd, $^3J_{HH} = 7.5$ Hz, $^4J_{HH} = 4.8$ Hz, $^5J_{HH} = 1.2$ Hz, $H_{bipy}$, 1H), 7.26 (ddd, $^3J_{HH} = 8.0$ Hz, $^3J_{HH} = 7.5$ Hz, $^5J_{HH} = 1.8$ Hz, $H_{bipy}$, 1H), 7.67 (dd, $^3J_{HH} = 8.3$ Hz, $^5J_{HH} = 2.3$ Hz, $H_{bipy}$, 1H), 8.59 (ddd, $^4J_{HH} = 4.8$ Hz, $^5J_{HH} = 1.8$ Hz, $^5J_{HH} = 0.9$ Hz, $H_{bipy}$, 1H), 8.80 (dd, $^3J_{HH} = 6.5$ Hz, $^5J_{HH} = 1.0$ Hz, $H_{bipy}$, 1H), 8.83 (dt, $^3J_{HH} = 7.1$ Hz, $^5J_{HH} = 1.1$ Hz, $H_{bipy}$, 1H) and 8.99 (dd, $^4J_{HH} = 2.3$ Hz, $^5J_{HH} = 0.8$ Hz, $H_{bipy}$, 1H) ppm. $^{13}$C {$^1$H} NMR ($C_6D_6$, 75.47 MHz): $\delta = 25.12$ (s, $CH_3$, 4 C), 67.39 (s, $CH_{Cp}$, 2 C), 70.23 (s, $CH_{Cp}$, 2 C), 74.26 (s, $CH_{Cp}$, 2 C), 76.29 (s, $CH_{Cp}$, 2 C), 82.62 (s, $C_{Cp}$, 1 C), 83.29 (s, $CCH_3$, 2 C), 120.96 (s, $CH_{bipy}$, 1 C), 120.99 (s, $CH_{bipy}$, 1 C), 123.38 (s, $CH_{bipy}$, 1 C), 134.36 (s, $CH_{bipy}$, 1 C), 135.63 (s, $C_{bipy}$, 1 C), 136.63 (s, $CH_{bipy}$, 1 C), 147.30 (s, $CH_{bipy}$, 1 C), 149.42 (s, $CH_{bipy}$, 1 C), 154.38 (s, $C_{bipy}$, 1 C) and 156.95 (s, $C_{bipy}$, 1 C) ppm. $^{11}$B NMR ($C_6D_6$, 96.29 MHz): $\delta = 33.11$ ppm. IR-ATR ($cm^{-1}$): $\tilde{\nu} = 3088$ (vw), 3049 (vw), 2975 (vw), 2927 (vw), 1651 (vw), 1586 (vw), 1572 (vw), 1551 (w), 1502 (m), 1484 (s), 1468 (m), 1444 (w), 1432 (w), 1381 (m), 1368 (m), 1323 (s), 1296 (m), 1276 (w), 1246 (vw), 1216 (vw), 1194 (vw), 1166 (vw), 1147 (m), 1127 (vs), 1093 (w), 1053 (vw), 1027 (w), 1000 (vw), 990 (vw), 965 (w), 904 (w), 889 (w), 853 (s), 823 (m), 797 (m), 773 (vw), 748 (s), 710 (vw), 693 (m), 669 (vw), 653 (vw), 639 (w), 616 (vw), 600 (vw), 580 (vw), 558 (vw), 520 (m), 494 (m), 483 (w), 464 (w), 441 (vw), 400 (m). EA [%] $C_{26}H_{27}BFeN_2O_2$ calc. (found): C 66.99 (67.08), H 5.84 (5.863), N 6.01 (5.78). APCI-MS (m/z): calc. 466.15, found. 467.7 $[M+H]^+$.

Synthesis of the metalloligands **2A**–**C**: **2A**: 1,1′-Fc(bipy)(Bpin) (300 mg, 0.644 mmol) and [Pd(dppf)$Cl_2$] (70 mg, 0.096 mmol) in a Schlenk flask are dissolved in 15 mL DME and 15 mL 1,4-dioxane and 4-trifluoromethylbromobenzene (0.3 mL, 480 mg, 2.133 mmol) was added. Then, 3 mL of a degassed aqueous solution of $Na_2CO_3$ (1 M) and 1 mL of a degassed aqueous solution of NaOH (3 M) were added and the reaction mixture was heated to 85 °C for 5 days. After cooling to room temperature, the reaction mixture was added on ice and extracted with EtOAc. The organic layer was washed with a saturated aqueous solution of $NH_4Cl$, water and brine and dried over $MgSO_4$. After removing all volatile components the crude product was purified by column chromatography (silica gel, $CH_2Cl_2$:EtOAc, first 1:0 then 0:1). The product was obtained as a dark orange solid. Yield: 234 mg (75 %). Mp. (sealed tube): 201 °C (decomposition). $^1$H NMR ($CD_2Cl_2$, 300.13 MHz): $\delta$ = 4.36 (dt, $^3J_{HH}$ = 2.2 Hz, $^3J_{HH}$ = 1.7 Hz, $H_{Cp}$, 4H), 4.64 (ddd, $^3J_{HH}$ = 3.8 Hz, $^3J_{HH}$ = 1.7 Hz, $H_{Cp}$, 4H), 7.31 (ddd, $^3J_{HH}$ = 7.5 Hz, $^4J_{HH}$ = 4.8 Hz, $^5J_{HH}$ = 1.2 Hz, $H_{bipy}$, 1H), 7.33 (s, $H_{Ph}$, 4H), 7.56 (dd, $^3J_{HH}$ = 8.3 Hz, $^5J_{HH}$ = 2.3 Hz, $H_{bipy}$, 1H), 7.82 (ddd, $^3J_{HH}$ = 8.0 Hz, $^3J_{HH}$ = 7.5 Hz, $^5J_{HH}$ = 1.8 Hz, $H_{bipy}$, 1H), 8.17 (dd, $^5J_{HH}$ = 8.3 Hz, $^5J_{HH}$ = 0.8 Hz, $H_{bipy}$, 1H), 8.38 (dt, $^3J_{HH}$ = 8.0 Hz, $^5J_{HH}$ = 1.1 Hz, $H_{bipy}$, 1H), 8.54 (dd, $^4J_{HH}$ = 2.4 Hz, $^5J_{HH}$ = 0.8 Hz, $H_{bipy}$, 1H) and 8.64 (ddd, $^4J_{HH}$ = 4.8 Hz, $^5J_{HH}$ = 1.8 Hz, $^5J_{HH}$ = 1.0 Hz, $H_{bipy}$, 1H) ppm. $^{13}$C{$^1$H} NMR ($CD_2Cl_2$, 75.47 MHz): $\delta$ = 68.20 (s, $CH_{Cp}$, 2 C), 68.59 (s, $CH_{Cp}$, 2 C), 71.71 (s, $CH_{Cp}$, 2 C), 71.76 (s, $CH_{Cp}$, 2 C), 83.10 (s, $C_{Cp}$, 1 C), 84.78 (s, $C_{Cp}$, 1 C), 120.87 (s, $CH_{bipy}$, 1 C), 120.99 (s, $CH_{bipy}$, 1 C), 123.89 (s, $CH_{bipy}$, 1 C), 125.72 (d, $^1J_{CF}$ = 345.30 Hz, $CF_3$, 1 C), 125.72 (q, $^3J_{CF}$ = 3.8 Hz, $CH_{Ph}$, 1 C), 126.32 (s, $CH_{Ph}$, 1 C), 127.48 (d, $^2J_{CF}$ = 105.3 Hz, $CCF_3$, 1 C) 133.83 (s, $CH_{bipy}$, 1 C), 134.08 (s, $C_{bipy}$, 1 C), 137.23 (s, $CH_{bipy}$, 1 C), 142.27 (s, $C_{Ph}$, 1 C), 146.88 (s, $CH_{bipy}$, 1 C), 149.62 (s, $CH_{bipy}$, 1 C), 153.94 (s, $C_{bipy}$, 1 C) and 156.59 (s, $C_{bipy}$, 1 C) ppm. $^{19}$F NMR ($CD_2Cl_2$, 282.40 MHz): δ = −62.76 ppm. IR-ATR ($cm^{-1}$): $\tilde{\nu}$ = 3079 (vw), 3053 (vw), 3005 (vw), 2045 (vw), 1613 (w), 1590 (w), 1574 (vw), 1555 (vw), 1532 (vw), 1508 (vw), 1469 (w), 1444 (w), 1435 (w), 1422 (w), 1402 (vw), 1388 (vw), 1321 (vs), 1284 (w), 1247 (vw), 1220 (vw), 1192 (vw), 1162 (s), 1144 (w), 1108 (vs), 1060 (s), 1036 (m), 1015 (w), 993 (vw), 957 (vw), 923 (vw), 890 (w), 842 (vs), 811 (m), 795 (m), 773 (vw), 745 (vs), 714 (vw), 697 (w), 686 (w), 642 (w), 619 (vw), 595 (vw), 570 (vw), 544 (vw), 520 (m), 508 (s), 493 (w), 476 (w), 460 (vw), 431 (w), 403 (w), 387 (vw). EA [%] $C_{27}H_{19}F_3FeN_2$ calc. (found): 66.96 (67.14), 3.95 (3.738), 5.78 (5.92). APCI-MS (m/z): calc. 484.08, found. 485.5 $[M+H]^+$.

**2B**: 1,1′-Fc(bipy)(Bpin) (300 mg, 0.644 mmol) and [Pd(dppf)$Cl_2$] (70 mg, 0.096 mmol) in a Schlenk flask are solved in 15 mL DME and 15 mL 1,4-dioxane. Then, 3,5-bis(trifluoromethyl)bromobenzene (0.3 mL, 510 mg, 1.764 mmol) was added. Afterwards, 3 mL of a degassed aqueous solution of $Na_2CO_3$ (1 M) and 1 mL of a degassed aqueous solution of NaOH (3 M) were added and the reaction mixture was heated to 85 °C for 5 days. After cooling to room temperature, the reaction mixture was added on ice and extracted with EtOAc. The organic layer was washed with a saturated aqueous solution of $NH_4Cl$, water and brine and dried over $MgSO_4$. After removing all volatile components the crude product was purified by column chromatography (silica gel, $CH_2Cl_2$:EtOAc, first 1:0 then 0:1). The product was obtained as a dark orange solid. Yield: 328 mg (92 %). Mp. (sealed tube): 130 °C; $^1$H NMR ($CD_2Cl_2$, 300.13 MHz): $\delta$ = 4.37–4.41 (m, $H_{Cp}$, 2H), 4.42–4.46 (m, $H_{Cp}$, 2H), 4.67–4.72 (m, $H_{Cp}$, 4H), 7.31 (ddd, $^3J_{HH}$ = 7.5 Hz, $^4J_{HH}$ = 4.8 Hz, $^5J_{HH}$ = 1.2 Hz, $H_{bipy}$, 1H), 7.45 (s, $H_{Ph}$, 1H), 7.51 (dd, $^3J_{HH}$ = 8.3 Hz, $^5J_{HH}$ = 2.3 Hz, $H_{bipy}$, 1H), 7.59 (s, $H_{Ph}$, 2H), 7.82 (ddd, $^3J_{HH}$ = 8.0 Hz, $^3J_{HH}$ = 7.5 Hz, $^5J_{HH}$ = 1.8 Hz, $H_{bipy}$, 1H), 8.14 (dd, $^5J_{HH}$ = 8.3 Hz, $^5J_{HH}$ = 0.8 Hz, $H_{bipy}$, 1H), 8.37 (dt, $^3J_{HH}$ = 8.0 Hz, $^5J_{HH}$ = 1.1 Hz, $H_{bipy}$, 1H), 8.46 (dd, $^4J_{HH}$ = 2.4 Hz, $^5J_{HH}$ = 0.8 Hz, $H_{bipy}$, 1H) and 8.64 (ddd, $^4J_{HH}$ = 4.8 Hz, $^5J_{HH}$ = 1.8 Hz, $^5J_{HH}$ = 0.9 Hz, $H_{bipy}$, 1H) ppm. $^{13}$C{$^1$H} NMR ($CD_2Cl_2$, 75.47 MHz): $\delta$ = 68.11 (s, $CH_{Cp}$, 2 C), 68.32 (s, $CH_{Cp}$, 2 C), 71.70 (s, $CH_{Cp}$, 2 C), 72.09 (s, $CH_{Cp}$, 2 C), 83.34 (s, $C_{Cp}$, 1 C), 83.47 (s, $C_{Cp}$, 1 C), 119.74 (s, $CH_{Ph}$, 2 C), 120.83 (s, $CH_{bipy}$, 1 C), 120.96 (s, $CH_{bipy}$, 1 C), 123.11 (d, $^1J_{CF}$ = 273.6 Hz, $CF_3$, 1 C), 123.91 (s, $CH_{bipy}$, 1 C), 125.84 (s, $CH_{Ph}$, 1 C), 131.93 (q, $^2J_{CF}$ = 32.9 Hz, $CCF_3$, 2 C), 133.11 (s, $C_{Ph}$, 1 C), 133.62 (s, $CH_{bipy}$, 1 C), 137.18 (s, $CH_{bipy}$, 1 C), 140.98 (s, $C_{bipy}$, 1 C), 146.82 (s, $CH_{bipy}$, 1 C), 149.60 (s, $CH_{bipy}$, 1 C), 154.00 (s, $C_{bipy}$, 1 C), 156.50 (s, $C_{bipy}$, 1 C) ppm. $^{19}$F NMR ($CD_2Cl_2$, 282.40 MHz): $\delta$ = −63.41 ppm. IR-ATR ($cm^{-1}$): $\tilde{\nu}$ = 3098 (vw), 3055 (vw), 1615 (vw), 1587 (vw), 1571 (vw), 1551 (vw), 1503 (vw), 1466 (vw), 1444 (vw), 1434 (w), 1389 (w), 1374 (vw), 1358 (m), 1271 (vs), 1167 (s), 1126 (vs), 1105 (m), 1091 (m), 1060 (vw), 1040 (w), 1027 (w), 999 (vw), 980 (vw), 967 (vw), 934 (vw), 915 (vw), 903 (vw), 883 (m), 857 (w), 844 (w), 836 (w), 822 (m), 797 (m), 773 (vw), 749 (s), 697 (s), 680 (s), 639 (w), 617 (vw), 560 (vw), 529 (w), 513 (m), 496 (m), 477 (w), 459 (vw), 448 (vw), 428 (vw), 416 (m), 404 (m). EA [%] $C_{28}H_{18}F_6FeN_2$ calc. (found): C 60.59 (60.43), H 3.29 (3.02), N 5.07 (4.60). APCI-MS (m/z): calc. 552.07, found. 553.8 $[M+H]^+$.

**2 C**: 1,1′-Fc(bipy)(Bpin) (300 mg, 0.644 mmol), [Pd(dppf)$Cl_2$] (70 mg, 0.096 mmol) and 4-nitrobromobenzene (130 mg, 0.644 mmol) in a Schlenk flask were dissolved in 15 mL DME and 15 mL 1,4-dioxane. Then, 3 mL of a degassed aqueous solution of $Na_2CO_3$ (1 M) and 1 mL of a degassed aqueous solution of NaOH (3 M) were added and the reaction mixture was heated to 85 °C for 5 days. After cooling to room temperature, the reaction mixture was added on ice and extracted with EtOAc. The organic layer was washed with a saturated aqueous solution of $NH_4Cl$, water and brine and dried over $MgSO_4$. After removing all volatile components, the crude product was resolved in $CH_2Cl_2$ and filtered over silica gel and the solvent was removed. Traces of 1,1′-Fc(bipy)(Bpin) were removed with hexane. The product was obtained as dark orange solid. Yield: 168 g (56 %). Mp. (sealed tube): 240 °C (decomposition). $^1$H NMR ($CD_2Cl_2$, 300.13 MHz): $\delta$ = 4.39 (dd, $^3J_{HH}$ = 2.1 Hz, $^3J_{HH}$ = 1.7 Hz, $H_{Cp}$, 2H), 4.47 (dd, $^3J_{HH}$ = 2.1 Hz, $^3J_{HH}$ = 1.7 Hz, $H_{Cp}$, 2H), 4.67–4.75 (m, $H_{Cp}$, 4H), 7.19–7.24 (m, $H_{Ph}$, 2H), 7.31 (ddd, $^3J_{HH}$ = 7.5 Hz, $^4J_{HH}$ = 4.8 Hz, $^5J_{HH}$ = 1.2 Hz, $H_{bipy}$, 1H), 7.48 (dd, $^3J_{HH}$ = 8.3 Hz, $^5J_{HH}$ = 2.3 Hz, $H_{bipy}$, 1H), 7.75–7.87 (m, $H_{Ph}$, 2 H, $H_{bipy}$, 1H)), 8.09 (dd, $^5J_{HH}$ = 8.3 Hz, $^5J_{HH}$ = 0.8 Hz, $H_{bipy}$, 1H), 8.30 (dt, $^3J_{HH}$ = 8.0 Hz, $^5J_{HH}$ = 1.1 Hz, $H_{bipy}$, 1H), 8.42 (dd, $^4J_{HH}$ = 2.3 Hz, $^5J_{HH}$ = 0.8 Hz, $H_{bipy}$, 1H) und 8.63 (ddd, $^4J_{HH}$ = 4.8 Hz, $^5J_{HH}$ = 1.8 Hz, $^5J_{HH}$ = 0.9 Hz, $H_{bipy}$, 1H) ppm. $^{13}$C{$^1$H} NMR ($CD_2Cl_2$, 75.47 MHz): $\delta$ = 68.03 (s, $CH_{Cp}$, 2 C), 68.73 (s, $CH_{Cp}$, 2 C), 71.65 (s, $CH_{Cp}$, 2 C), 72.30 (s, $CH_{Cp}$, 2 C), 83.48 (s, $C_{Cp}$, 1 C), 83.65 (s, $C_{Cp}$, 1 C), 120.79 (s, $CH_{bipy}$, 1 C), 120.86 (s, $CH_{bipy}$, 1 C), 123.96 (s, $CH_{bipy}$, 1 C), 124.22 (s, $CH_{Ph}$, 2 C), 126.26 (s, $CH_{Ph}$, 2 C), 133.00 (s, $C_{Ph}$, 1 C), 133.66 (s, $CH_{bipy}$, 1 C), 137.32 (s, $CH_{bipy}$, 1 C), 145.62 (s, $C_{bipy}$, 1 C), 146.82 (s, $CH_{bipy}$, 1 C), 153.89 (s, $C_{bipy}$, 1 C), 156.33 (s, $C_{bipy}$, 1 C) ppm. IR-ATR ($cm^{-1}$): $\tilde{\nu}$ = 3082 (vw), 3056 (vw), 3003 (vw), 2916 (vw), 2820 (vw), 2430 (vw), 1997 (vw), 1919 (vw), 1815 (vw), 1635 (vw), 1591 (s), 1555 (w), 1504 (vs), 1467 (w), 1445 (w), 1435 (w), 1402 (vw), 1389 (w), 1325 (vs), 1286 (s), 1248 (w), 1184 (vw), 1148 (vw), 1129 (vw), 1107 (m), 1083 (w), 1058 (vw), 1034 (m), 1009 (w), 992 (w), 926 (vw), 908 (vw), 891 (w), 844 (vs), 819 (m), 794 (s), 774 (vw), 744 (vs), 708 (w), 691 (m), 679 (w), 651 (vw), 639 (w), 618 (vw), 593 (vw), 557 (vw), 535 (w), 521 (s), 501 (s), 481 (m), 461 (w), 433 (w), 400 (w), 385 (w). EA [%] $C_{26}H_{19}FeN_3O_2$ calc. (found): C 67.70 (67.50), H 4.15 (4.05), N 9.11 (9.05). APCI-MS (m/z): calc. 461.05, found 462.7 $[M+H]^+$.

General synthesis of the Pd complexes **3A**–**C**: The respective ligand (0.093 mmol) and [Pd(cod)$Cl_2$] (0.093 mmol) were dissolved in $CH_2Cl_2$ (10 mL) and stirred overnight. The solution turned dark red. After removing all volatiles, the residue was dissolved in $CH_2Cl_2$ and after adding hexane as antisolvent crystals could be obtained. **3A**: Yield: 91 %. Mp (sealed tube under argon): decomposition, due to the dark colour of the compound no exact temperature can be specified. $^1$H NMR ($CD_2Cl_2$, 300.13 MHz): δ = 4.45 (dd, $^3J_{HH}$ = 2.2, $^3J_{HH}$ = 1.7 Hz, $H_{Cp}$, 2H), 4.55 (dd, $^3J_{HH}$ = 2.2, $^3J_{HH}$ = 1.7 Hz, $H_{Cp}$, 2H), 4.76–4.79 (m, $H_{Cp}$, 2H), 4.82–4.85 (m, $H_{Cp}$, 2H), 7.24–7.25 (m, $H_{bipy}$, 1H), 7.27–7.28 (m, $H_{bipy}$, 1H), 7.37–7.43 (m, $H_{Ph}$, 4H), 7.55 (ddd, $^3J_{HH}$ = 7.6, $^4J_{HH}$ = 5.8, $^5J_{HH}$ = 1.4 Hz, $H_{bipy}$, 1H), 7.82 (d, $^3J_{HH}$ = 8.0 Hz, $H_{bipy}$, 1H),

8.07 (ddd, $^3J_{HH}$ = 8.1, $^3J_{HH}$ = 7.6, $^5J_{HH}$ = 1.6 Hz, $H_{bipy}$, 1H), 9.12 (dd, $^5J_{HH}$ = 1.7, $^5J_{HH}$ = 0.9 Hz, $H_{bipy}$, 1H), 9.34 (ddd, $^4J_{HH}$ = 5.9, $^5J_{HH}$ = 1.6, $^5J_{HH}$ = 0.6 Hz, $H_{bipy}$, 1H) ppm. $^{19}$F NMR ($CD_2Cl_2$, 282.40 MHz): $\delta$ = −62.69 ppm. IR-ATR ($cm^{-1}$): $\tilde{\nu}$ = 3071 (vw), 2188 (vw), 2160 (vw), 2032 (vw), 1983 (vw), 1611 (w), 1594 (w), 1577 (vw), 1563 (w), 1515 (vw), 1473 (m), 1439 (w), 1421 (w), 1389 (vw), 1321 (vs), 1284 (m), 1244 (w), 1214 (vw), 1192 (vw), 1164 (s), 1122 (s), 1106 (vs), 1089 (m), 1057 (s), 1038 (w), 1012 (w), 954 (vw), 934 (vw), 895 (w), 845 (vs), 833 (m), 816 (m), 785 (m), 745 (w), 721 (m), 695 (w), 686 (w), 672 (vw), 646 (w), 634 (vw), 594 (w), 558 (vw), 533 (w), 520 (m), 510 (s), 483 (w), 441 (s), 414 (m), 399 (vw), 379 (w). EA [%] $C_{27}H_{19}Cl_2F_3FeN_2Pd$ calc. (found): 49.02 (49.13), 2.89 (3.14), 4.23 (4.59). **3B**: Yield: 92.5 %. Mp (sealed tube under argon): 300 °C (decomposition). $^1$H NMR ($CD_2Cl_2$, 300.13 MHz): $\delta$ = 4.48–4.50 (m, $H_{Cp}$, 2H)), 4.53 (dd, $^3J_{HH}$ = 2.2, $^3J_{HH}$ = 1.7 Hz, $H_{Cp}$, 2H), 4.76–4.80 (m, $H_{Cp}$, 4H), 7.54 (m, $H_{Ph}$, 1H), 7.55 (s, $H_{bipy}$, 1H), 7.56 (s, $H_{bipy}$, 1H), 7.57–7.60 (m, $H_{bipy}$, 1H), 7.65 (m, $H_{Ph}$, 1H), 7.88 (ddd, $^3J_{HH}$ = 8.0, $^5J_{HH}$ = 1.3, $^5J_{HH}$ = 0.6 Hz, $H_{bipy}$, 1H), 8.11 (ddd, $^3J_{HH}$ = 8.1, $^3J_{HH}$ = 7.6, $^5J_{HH}$ = 1.6 Hz, $H_{bipy}$, 1H), 9.33 (t, $^5J_{HH}$ = 1.4 Hz, $H_{bipy}$, 1H), 9.36 (ddd, $^4J_{HH}$ = 5.8, $^5J_{HH}$ = 1.6, $^5J_{HH}$ = 0.7 Hz, $H_{bipy}$, 1H) ppm. $^{19}$F NMR ($CD_2Cl_2$, 282.40 MHz): $\delta$ = −63.02 ppm. IR-ATR ($cm^{-1}$): $\tilde{\nu}$ = 3076 (vw), 3035 (vw), 1603 (w), 1578 (vw), 1566 (vw), 1518 (vw), 1498 (vw), 1475 (vw), 1440 (vw), 1389 (w), 1359 (m), 1282 (vs), 1248 (w), 1209 (vw), 1166 (s), 1117 (vs), 1090 (m), 1069 (vw), 1053 (vw), 1042 (vw), 1027 (w), 998 (vw), 921 (vw), 900 (vw), 882 (w), 854 (w), 844 (vw), 825 (m), 776 (w), 743 (w), 718 (w), 698 (m), 683 (s), 650 (vw), 616 (vw), 593 (vw), 561 (vw), 528 (vw), 509 (m), 498 (w), 480 (w), 457 (w), 425 (w), 414 (w), 407 (m). EA [%] $C_{28}H_{18}Cl_2F_6FeN_2Pd$ calc. (found): C 46.09 (46.12), H 2.49 (2.64), N 3.84 (3.65). **3C**: Yield: (92 %). Mp. (sealed tube under argon): decomposition, due to the dark color of the compound no exact temperature can be specified. $^1$H NMR ($CD_2Cl_2$, 300.13 MHz): $\delta$ = 4.54 (dd, $^3J_{HH}$ = 2.2 Hz, $^3J_{HH}$ = 1.7 Hz, $H_{Cp}$, 2H), 4.58 (dd, $^3J_{HH}$ = 2.2 Hz, $^3J_{HH}$ = 1.7 Hz, $H_{Cp}$, 2H), 4.81 (dd, $^3J_{HH}$ = 1.7 Hz, $H_{Cp}$, 2H), 4.85–4.87 (m, $H_{Cp}$, 2H), 7.17–7.23 (m, $H_{Ph}$, 2H), 7.41–7.49 (m, $H_{bipy}$, 2H) 7.58 (ddd, $^3J_{HH}$ = 7.6 Hz, $^4J_{HH}$ = 5.7 Hz, $^5J_{HH}$ = 1.4 Hz, $H_{bipy}$, 1H), 7.78 (ddd, $^3J_{HH}$ = 8.3 Hz, $^5J_{HH}$ = 1.3 Hz, $^5J_{HH}$ = 0.6 Hz $H_{bipy}$, 1H), 7.94–8.01 (m, $H_{Ph}$, 2 H, $H_{bipy}$, 1H)), 8.11 (ddd, $^3J_{HH}$ = 8.1 Hz, $^3J_{HH}$ = 87.6 Hz, $^5J_{HH}$ = 1.6 Hz, $H_{bipy}$, 1H), 9.00 (dd, $^4J_{HH}$ = 2.1 Hz, $^5J_{HH}$ = 0.6 Hz, $H_{bipy}$, 1H) und 9.34 (ddd, $^4J_{HH}$ = 5.7 Hz, $^5J_{HH}$ = 1.6 Hz, $^5J_{HH}$ = 0.7 Hz, $H_{bipy}$, 1H) ppm. IR-ATR ($cm^{-1}$): $\tilde{\nu}$ = 3081 (vw), 1663 (vw), 1593 (s), 1564 (w), 1502 (vs), 1472 (s), 1438 (w), 1384 (vw), 1325 (vs), 1285 (m), 1264 (w), 1246 (w), 1209 (vw), 1187 (vw), 1170 (vw), 1149 (vw), 1110 (m), 1083 (w), 1067 (vw), 1054 (vw), 1040 (w), 1028 (w), 1012 (vw), 930 (vw), 893 (m), 848 (s), 834 (m), 823 (s), 781 (s), 755 (m), 739 (s), 719 (m), 709 (w), 693 (s), 672 (vw), 652 (vw), 639 (vw), 556 (vw), 538 (m), 526 (m), 506 (s), 490 (m), 472 (w), 446 (s), 421 (w), 408 (w), 395 (w). EA [%] $C_{26}H_{19}Cl_2FeN_3O_2Pd \cdot {}^1/_3\ CH_2Cl_2$ calc. (found): C 47.40 (47.55), H 2.97 (2.88), N 6.30 (6.22).

General synthesis of the Cu complexes **4A**–**D**: The respective ligand (0.083 mmol) and $CuCl_2$ (0.083 mmol) were dissolved in $CH_2Cl_2$ (10 mL) and stirred overnight. The solution turned dark red. After removing all volatiles, the residue was washed with hexane in dried under vacuum. Data for compound **4A**: Yield: 78.3 %. Mp. (sealed tube under argon): 162 °C (decomposition). IR-ATR ($cm^{-1}$): $\tilde{\nu}$ = 3083 (vw), 2193 (vw), 2175 (vw), 2153 (vw), 2053 (vw), 1993 (vw), 1942 (vw), 1608 (w), 1598 (w), 1567 (vw), 1514 (vw), 1476 (w), 1458 (vw), 1438 (w), 1421 (vw), 1391 (vw), 1321 (vs), 1285 (w), 1249 (w), 1214 (vw), 1169 (m), 1110 (vs), 1091 (m), 1062 (m), 1038 (w), 1013 (w), 930 (vw), 897 (vw), 850 (m), 841 (m), 821 (w), 789 (m), 748 (w), 727 (m), 687 (w), 667 (vw), 643 (w), 596 (w), 555 (vw), 520 (w), 511 (w), 495 (w), 482 (vw), 468 (vw), 440 (w), 421 (w), 414 (w), 386 (w). EA [%] $C_{54}H_{38}Cl_4F_6Cu_2Fe_2N_4 \cdot {}^1/_2\ C_6H_{14}$ calc. (found): C 51.14 (51.06), H 3.07 (3.06), N 4.38 (3.67). Data for compound **4B**: Yield: 86.5 %. Mp (sealed tube under argon): 190 °C (decomposition). IR-ATR ($cm^{-1}$): $\tilde{\nu}$ = 3085 (vw), 3038 (vw), 2223 (vw), 2192 (vw), 2028 (vw), 1601 (vw), 1582 (vw), 1570 (vw), 1500 (vw), 1479 (vw), 1439 (vw), 1387 (w), 1360 (m), 1334 (vw), 1314 (vw), 1279 (vs), 1253 (vw), 1179 (m), 1120 (vs), 1105 (w), 1091 (w), 1071 (vw), 1060 (vw), 1049 (vw), 1025 (w), 1000 (vw), 898 (vw), 882 (w), 845 (vw), 829 (w), 805 (vw), 789 (w), 774 (vw), 750 (w), 728 (w), 698 (m), 683 (m), 642 (vw), 618 (vw), 593 (vw), 569 (vw), 524 (vw), 511 (m), 495 (w), 477 (w), 457 (vw), 421 (w), 415 (w), 403 (w), 382 (vw). EA [%] $C_{56}H_{36}Cl_4F_{12}Cu_2Fe_2N_4$ calc. (found): C 48.97 (48.68), H 2.64 (2.73), N 4.08 (4.10). **4C**: Yield: 74 %. Mp (sealed tube under argon): 180 °C (decomposition). IR-ATR ($cm^{-1}$): $\tilde{\nu}$ = 3081 (vw), 2226 (vw), 2206 (vw), 2190 (vw), 2164 (vw), 2153 (vw), 2141 (vw), 2058 (vw), 2039 (vw), 2027 (vw), 2019 (vw), 2008 (vw), 1992 (vw), 1972 (vw), 1860 (vw), 1595 (s), 1567 (vw), 1510 (vs), 1477 (m), 1440 (w), 1409 (vw), 1385 (vw), 1332 (vs), 1287 (w), 1248 (vw), 1211 (vw), 1170 (w), 1148 (vw), 1111 (w), 1084 (vw), 1064 (vw), 1049 (w), 1037 (w), 1022 (vw), 961 (vw), 929 (vw), 894 (w), 869 (vw), 849 (m), 821 (w), 791 (m), 749 (m), 727 (m), 693 (w), 668 (w), 642 (vw), 617 (vw), 586 (vw), 556 (vw), 526 (m), 508 (m), 488 (m), 468 (w), 451 (m), 438 (w), 419 (m), 407 (m), 396 (w). EA [%] $C_{52}H_{38}Cl_4Cu_2Fe_2N_6O_4$ calc. (found): C 52.42 (52.24), H 3.21 (3.44), N 6.52 (7.05). **4D**: Yield: 76.5 %. Mp (sealed tube under argon): 180 °C (decomposition). IR-ATR ($cm^{-1}$): $\tilde{\nu}$ = 3103 (vw), 3084 (vw), 3053 (vw), 3037 (vw), 2219 (vw), 2196 (vw), 2060 (vw), 1602 (m), 1582 (vw), 1570 (w), 1507 (vw), 1479 (m), 1438 (m), 1409 (vw), 1401 (vw), 1376 (vw), 1334 (vw), 1312 (w), 1285 (w), 1252 (w), 1203 (vw), 1168 (m), 1137 (w), 1105 (w), 1093 (w), 1062 (w), 1047 (m), 1036 (w), 1021 (w), 1002 (w), 953 (vw), 895 (w), 873 (m), 847 (m), 825 (m), 801 (m), 788 (s), 749 (vs), 729 (vs), 694 (vw), 669 (vw), 653 (vw), 641 (vw), 592 (vw), 571 (vw), 523 (w), 512 (vs), 489 (vs), 473 (s), 451 (m), 430 (s), 420 (s), 401 (m). EA [%] $C_{40}H_{32}Cl_4Cu_2Fe_2N_4 \cdot {}^1/_3\ C_6H_{14}$ calc. (found): C 51.58 (51.90), H 3.78 (3.51), N 5.73 (6.10).

General synthesis of the Ni complexes **5A**, **5B** and **5D**: The respective ligand (0.165 mmol) and $[(PPh_3)_2NiMesBr_{0.8}/Cl_{0.2}]$ (0.165 mmol) were dissolved in $CH_2Cl_2$ (10 mL) and stirred overnight. The solution turned red. After removing all volatiles, the residue was washed with hexane to remove $PPh_3$. Afterwards the compound was dried under vacuum. **5A**: Yield: 85.6 %. Mp. (sealed tube under argon): 185 °C (decomposition).$^1$H NMR ($CD_2Cl_2$, 300.13 MHz): $\delta$ = *SP*-4-3: 2.27 (s, Mes-*p*-C$H_3$, 3H), 3.15 (s, Mes-*o*-C$H_3$, 6H), 4.44 (t, $^3J_{HH}$ = 1.9 Hz, $H_{Cp}$, 2H), 4.49 (t, $^3J_{HH}$ = 1.9 Hz, $H_{Cp}$, 2H), 4.74–4.80 (m, $H_{Cp}$, 2H), 4.84 (t, $^3J_{HH}$ = 1.9 Hz, $H_{Cp}$, 2H), 6.57 (s, $H_{Mes}$, 2H), 7.0–8.0 (several overlaying multiplets, $H_{bipy}$ + $H_{Ph}$, 10H), 9.34 (s, $H_{bipy}$, 1H) ppm; *SP*-4-2: 2.39 (s, Mes-*p*-C$H_3$, 3H), 3.21 (s, Mes-*o*-C$H_3$, 6H), 4.19 (t, $^3J_{HH}$ = 1.9 Hz, $H_{Cp}$, 2H), 4.20–4.28 (m, $H_{Cp}$, 2H), 4.26–4.34 (m, $H_{Cp}$, 2H), 4.55 (t, $^3J_{HH}$ = 2.0 Hz, $H_{Cp}$, 2H), 6.73 (s, $H_{Mes}$, 2H), 7.0–8.0 (several overlaying multiplets, $H_{bipy}$ + $H_{Ph}$, 10H), 9.39 (d, $^4J_{HH}$ = 5.4 Hz, $H_{bipy}$, 1H) ppm. The evaluation of the chloride species is not included. Due to the overlay of several species, the $^{13}$C NMR spectra were not evaluated.

$^{19}$F-NMR ($CD_2Cl_2$, 282.40 MHz): $\delta$ = *SP*-4-3: −62.66; *SP*-4-2: −62.61 ppm. IR-ATR ($cm^{-1}$): $\tilde{\nu}$ = 3082 (vw), 2913 (vw), 2198 (vw), 2147 (vw), 2044 (vw), 2004 (vw), 1979 (vw), 1614 (w), 1600 (w), 1565 (vw), 1508 (vw), 1476 (w), 1436 (w), 1422 (w), 1407 (w), 1382 (vw), 1325 (vs), 1285 (w), 1247 (vw), 1214 (vw), 1194 (vw), 1155 (m), 1110 (vs), 1090 (m), 1063 (m), 1035 (vw), 1017 (w), 938 (vw), 895 (w), 844 (s), 815 (m), 788 (m), 746 (s), 725 (w), 692 (m), 645 (vw), 633 (vw), 595 (vw), 560 (vw), 533 (vw), 511 (s), 499 (m), 484 (w), 456 (vw), 440 (w), 393 (vw). EA [%] $C_{36}H_{30}FeN_2NiF_3Br_{0.8}Cl_{0.2}$ calc. (found): C 58.97 (59.83), H 4.12 (3.86), N 3.82 (3.54). **5B**: Yield: 94.6 %. Mp (sealed tube under argon): 200 °C (decomposition). $^1$H NMR ($CD_2Cl_2$, 300.13 MHz): $\delta$ = *SP*-4-3: 2.25 (s, Mes-*p*-C$H_3$, 3H), 3.09 (s, Mes-*o*-C$H_3$, 6H), 4.45–4.47 (m, $H_{Cp}$, 2H), 4.48–4.50 (m, $H_{Cp}$, 2H), 4.74–4.77 (m, $H_{Cp}$, 2H), 4.78–4.80 (m, $H_{Cp}$, 2H), 6.53–6.55 (m, $H_{Mes}$, 2H), 7.0–8.1 (several overlaying multiplets, $H_{bipy}$ + $H_{Ph}$, 9H), 9.48 (dd, $^4J_{HH}$ = 2.1 Hz, $^5J_{HH}$ = 0.8 Hz, $H_{bipy}$, 1H) ppm; *SP*-4-2: 2.37 (s, Mes-*p*-C$H_3$, 3H), 3.18 (s,Mes-*o*-C$H_3$, 6H), 4.16 (dd, $^4J_{HH}$ = 2.2, 1.7 Hz, $H_{Cp}$, 2H), 4.23–4.25 (m, $H_{Cp}$, 2H), 4.28–4.30 (m, $H_{Cp}$, 2H), 4.51 (dd, $^3J_{HH}$ = 1.8 Hz, $H_{Cp}$, 2H), 6.70–6.72 (m,

Research Article
doi.org/10.1002/ejic.202100898



$H_{Mes}$, 2H), 7.0–8.1 (several overlaying multiplets, $H_{bipy}+H_{Ph}$, 9H), 9.41 (ddd, $^4J_{HH}=5.5$ Hz, $^5J_{HH}=1.7$ Hz, $^5J_{HH}=0.8$ Hz, $H_{bipy}$, 1H) ppm. The evaluation of the chloride species is not included. Due to the overlay of several species, the $^{13}$C NMR spectra were not evaluated. $^{19}$F NMR ($CD_2Cl_2$, 282.40 MHz): $\delta = SP$-4-3: −63.16; *SP*-4-2: −63.23 ppm. IR-ATR ($cm^{-1}$): $\tilde{\nu}=3054$ (vw), 2925 (vw), 2223 (vw), 2065 (vw), 2035 (vw), 2004 (vw), 1947 (vw), 1597 (vw), 1577 (vw), 1563 (vw), 1498 (vw), 1474 (vw), 1435 (w), 1407 (vw), 1384 (w), 1358 (m), 1311 (vw), 1269 (vs), 1196 (m), 1167 (m), 1125 (vs), 1106 (w), 1092 (w), 1050 (vw), 1024 (w), 999 (vw), 887 (w), 848 (w), 826 (w), 790 (vw), 775 (vw), 750 (w), 726 (vw), 696 (s), 682 (m), 652 (vw), 616 (vw), 563 (vw), 520 (s), 512 (s), 498 (m), 459 (vw), 417 (w), 396 (w). EA [%] $C_{37}H_{29}FeN_2NiF_6Br_{0.8}Cl_{0.2}\cdot{}^1/_2\ C_6H_{14}$ calc. (found.): C 56.90 (57.06), H 4.30 (4.18), N 3.32 (3.36). **5D**: Yield: 85.6%. Mp. (sealed tube under argon): 185 °C (decomposition). $^1$H NMR ($CD_2Cl_2$, 300.13 MHz): $\delta = SP$-4-3: 2.27 (s, Mes-*p*-$CH_3$, 3H), 3.15 (s, Mes-*o*-$CH_3$, 6H), 4.44 (t, $^3J_{HH}=1.9$ Hz, $H_{Cp}$, 2H), 4.49 (t, $^3J_{HH}=1.9$ Hz, $H_{Cp}$, 2H), 4.74–4.80 (m, $H_{Cp}$, 2H), 4.84 (t, $^3J_{HH}=1.9$ Hz, $H_{Cp}$, 2H), 6.57 (s, $H_{Mes}$, 2H), 7.0–8.0 (several overlaying multiplets, $H_{bipy}+H_{Ph}$, 10H), 9.34 (s, $H_{bipy}$, 1H) ppm; *SP*-4-2: 2.39 (s, Mes-*p*-$CH_3$, 3H), 3.21 (s, Mes-*o*-$CH_3$, 6H), 4.19 (t, $^3J_{HH}=1.9$ Hz, $H_{Cp}$, 2H), 4.20–4.28 (m, $H_{Cp}$, 2H), 4.26–4.34 (m, $H_{Cp}$, 2H), 4.55 (t, $^3J_{HH}=2.0$ Hz, $H_{Cp}$, 2H), 6.73 (s, $H_{Mes}$, 2H), 7.0–8.0 (several overlaying multiplets, $H_{bipy}+H_{Ph}$, 10H), 9.39 (d, $^4J_{HH}=5.4$ Hz, $H_{bipy}$, 1H) ppm. The evaluation of the chloride species is not included. Due to the overlay of several species, the $^{13}$C NMR spectra were not evaluated. $^{19}$F NMR ($CD_2Cl_2$, 282.40 MHz): $\delta = SP$-4-3: −62.66; *SP*-4-2: −62.61 ppm. IR-ATR ($cm^{-1}$): $\tilde{\nu}=3082$ (vw), 2913 (vw), 2198 (vw), 2147 (vw), 2044 (vw), 2004 (vw), 1979 (vw), 1614 (w), 1600 (w), 1565 (vw), 1508 (vw), 1476 (w), 1436 (w), 1422 (w), 1407 (w), 1382 (vw), 1325 (vs), 1285 (w), 1247 (vw), 1214 (vw), 1194 (vw), 1155 (m), 1110 (vs), 1090 (m), 1063 (m), 1035 (vw), 1017 (w), 938 (vw), 895 (w), 844 (s), 815 (m), 788 (m), 746 (s), 725 (w), 692 (m), 645 (vw), 633 (vw), 595 (vw), 560 (vw), 533 (vw), 511 (s), 499 (m), 484 (w), 456 (vw), 440 (w), 393 (vw). EA [%] $C_{36}H_{30}FeN_2NiF_3Br_{0.8}Cl_{0.2}$ calc. (found): C 58.97 (59.83), H 4.12 (3.86), N 3.82 (3.54).

General synthesis of the methoxides **6A**, **6B** and **6D**: The Ni compound (**5A**, **5B**, **5C**) (83.6 mmol) and sodium methoxides (278 mmol) were dissolved in methanol and stirred overnight. After 2 h the solution turns dark red. Afterwards the volatiles are removed under reduced pressure. The residue is dissolved in dichloromethane filtrated with the help of a syringe filter. After removing all volatiles, the products are obtained as dark red powders. **6A**: Yield: 61%. $^1$H NMR ($CD_2Cl_2$, 300.13 MHz): $\delta = SP$-4-3: 2.28 (s, Mes-*p*-$CH_3$, 3H), 2.60 (s, O$CH_3$, 3H), 3.17 (s, Mes-*o*-$CH_3$, 6H), 4.17–4.18 (m, $H_{Cp}$, 4H), 4.42–4.43 (m, $H_{Cp}$, 2H), 4.44–4.46 (m, $H_{Cp}$, 2H), 6.64 (s, $H_{Mes}$, 2H), 6.9–8.1 (several overlaying multiplets, $H_{bipy}+H_{Ph}$, 10H), 8.93 (dd, $^4J_{HH}=2.0$, 1.0 Hz, $H_{bipy}$, 1H) ppm; *SP*-4-2: 2.39 (s, Mes-*p*-$CH_3$, 3H), 2.68 (s, O$CH_3$, 3H), 3.27 (s, Mes-*o*-$CH_3$, 6H), 4.22 (dd, $^3J_{HH}=1.7$ Hz, $H_{Cp}$, 2H), 4.26 (dd, $^3J_{HH}=2.1$ Hz, 1.7 Hz, $H_{Cp}$, 2H), 4.52–4.55 (m, $H_{Cp}$, 2H), 4.79 (q, $^3J_{HH}=2.0$ Hz, $H_{Cp}$, 2H), 6.80 (s, $H_{Mes}$, 2H), 6.9–8.1 (several overlaying multiplets, $H_{bipy}+H_{Ph}$, 10H), 8.98 (dd, $^4J_{HH}=5.4$ Hz, $^5J_{HH}=1.7$ Hz, 0.8 Hz, $H_{bipy}$, 1H) ppm. **6B**: Yield: 53.6%.$^1$H NMR ($C_6D_6$, 300.13 MHz): $\delta = SP$-4-3: 2.46 (s, Mes-*p*-$CH_3$, 3H), 3.40 (s, O$CH_3$, 3H), 3.60 (s,Mes-*o*-$CH_3$, 6H), 3.93–4.02 (m, $H_{Cp}$, 4H), 4.15–4.18 (m, $H_{Cp}$, 2H), 4.33–4.37 (m, $H_{Cp}$, 2H), 6.5–8.1 (several overlaying multiplets, $H_{bipy}+H_{Ph}+H_{Mes}$, 11H), 9.49–9.60 (m, $H_{bipy}$, 1H) ppm; *SP*-4-2: 2.50 (s, Mes-*p*-$CH_3$, 3H), 3.54 (s, O$CH_3$, 3H), 3.60 (s, Mes-*o*-$CH_3$, 6H), 3.75–3.77 (m, $H_{Cp}$, 2H), 3.90–3.91 (m, $H_{Cp}$, 2H), 3.92–3.94 (m, $H_{Cp}$, 2H), 4.01–4.09 (m, $H_{Cp}$, 2H), 5.92 (ddd, $^3J_{HH}=6.9$ Hz, $^4J_{HH}=5.8$ Hz, $^5J_{HH}=2.0$ Hz, $H_{bipy}$, 2H), 7.0–8.1 (several overlaying multiplets, $H_{bipy}+H_{Ph}+H_{Mes}$, 10H), 9.49–9.60 (m, $H_{bipy}$, 1H) ppm. **6D**: Yield: 59%. $^1$H NMR ($CD_2Cl_2$, 300.13 MHz): $\delta = SP$-4-3: 2.26 (s, Mes-*p*-$CH_3$, 3H), 2.54 (s, O$CH_3$, 3H), 3.13 (s,Mes-*o*-$CH_3$, 6H), 4.14 (s, $H_{Cp}$, 5H), 4.48 - 4.51 (m, $H_{Cp}$, 2H), 4.84–4.87 (m, $H_{Cp}$, 2H), 6.63 (s, $H_{Mes}$, 2H), 7.3–8.1 (several overlaying multiplets, $H_{bipy}$, 6H), 9.02 (dd, $^4J_{HH}=2.3$ Hz, $^5J_{HH}=2.3$ Hz, $H_{bipy}$, 1H) ppm; *SP*-4-2: 2.37 (s, Mes-*p*-$CH_3$, 3H), 2.62 (s, O$CH_3$, 3H), 3.20 (s,Mes-*o*-$CH_3$, 6H), 3.92 (s, $H_{Cp}$, 5H), 4.26 (dd, $^3J_{HH}=2.1$ Hz, 1.7 Hz, $H_{Cp}$, 2H), 4.33 (44, $^3J_{HH}=2.1$ Hz, 1.7 Hz, $H_{Cp}$, 2H), 6.76 (s, $H_{Mes}$, 2H), 7.3–8.1 (several overlaying multiplets, $H_{bipy}$, 6H), 8.98 (ddd, $^4J_{HH}=5.4$ Hz, $^5J_{HH}=1.7$ Hz, 0.8 Hz, $H_{bipy}$, 1H) ppm

## Crystal structure determinations

Crystal data collection and processing parameters are given below. In order to avoid degradation, single crystals were mounted in perfluoropolyalkyl ether oil on top of the edge of an open Mark tube and then brought into the cold nitrogen stream of a low-temperature device (Oxford Cryosystems Cryostream unit) so that the oil solidified. Diffraction data were measured on a Stoe IPDS II diffractometer using graphite-monochromated Mo-Kα (0.71073 Å) radiation, and corrected for absorption. The structures were solved by dual-space direct methods with SHELXT,[22] followed by full-matrix least-squares refinement using SHELXL-2018.[22] All non-hydrogen atoms were refined anisotropically, with hydrogen atoms placed in calculated positions using a riding model. In **1**, the expected disorder of the non-planar Bpin moiety was modelled with pairs of partial occupancy (54% and 46%) anisotropic oxygen and methyl carbon atoms, with similarity restraints applied to bond lengths as appropriate. In **2C**, two *para*-substituted aromatic rings showed correlated disorder involving rotation about their 1–4 axes, and were refined with pairs of partial occupancy (51.6% and 48.4%) anisotropic atoms without restraints, and common temperature factors assigned to the almost overlapping pairs of pivot atoms. The $-CF_3$ groups in **3A**, **4A** and **5A** are disordered, and were refined with pairs of partial occupancy anisotropic C and F atoms, with similarity restraints applied to bond lengths and rigid-bond restraints applied to the thermal parameters of these C and F atoms.

Although the bulk product of **5A** was shown by NMR to be a mixture of the bromide and chlorido complexes, corresponding to the Br/Cl mixture in the starting material, there was no evidence for any minor chlorido species in the crystal structure. The thermal parameters and form of the thermal ellipsoid for Br(1) are consistent with "pure" Br at this site.

Crystallographic data, data collection, and refinement details are summarized below.

**1**: $C_{26}H_{27}BFeN_2O_2$, 466.15 g mol$^{-1}$, monoclinic, $P2_1/n$, $a=1405.06(4)$, $b=1066.77(3)$, $c=1637.85(5)$ pm, $\beta=112.277(2)°$, $V=2271.70(12)$ $10^6$ pm$^3$, $T=200$ K, $Z=4$, $\mu$(Mo-$K\alpha$) = 0.690 mm$^{-1}$, $D_{calcd.}=$ 1.363 g cm$^{-3}$; crystal dimensions $0.25\times0.20\times0.15$ mm$^3$, 30167 reflections, 5865 unique data, $R_{int}=0.0350$; 352 parameters, 40 restraints, $wR_2$ (all data) = 0.0926, $S=1.036$ (all data), $R_1=0.0328$ (4669 data with $I>2\sigma(I)$), max/min residual electron density: +0.32/−0.37 e $10^{-6}$ pm$^{-3}$.

**2A**: $C_{27}H_{19}F_3FeN_2$, 484.29 g mol$^{-1}$, monoclinic, $P2_1/n$, $a=1581.9(2)$, $b=771.23(7)$, $c=1656.5(2)$ pm, $\beta=96.949(10)°$, $V=2006.2(4)$ $10^6$ pm$^3$, $T=100$ K, $Z=4$, $\mu$(Mo-$K\alpha$) = 0.799 mm$^{-1}$, $D_{calcd.}=$ 1.603 g cm$^{-3}$; crystal dimensions $0.15\times0.15\times0.01$ mm$^3$; 10126 reflections, 3646 unique data, $R_{int}=0.0570$; 298 parameters, 0 restraints, $wR_2$ (all data) = 0.2102, $S=1.080$ (all data), $R_1=0.0729$ (2520 data with $I>2\sigma(I)$), max/min residual electron density: +0.75/−0.55 e $10^{-6}$ pm$^{-3}$.

**2C**: $C_{26}H_{19}FeN_3O_2\cdot CH_2Cl_2$, 546.22 g mol$^{-1}$, triclinic, $P\bar{1}$, $a=757.36(4)$, $b=1041.83(5)$, $c=1614.63(7)$ pm, $\alpha=102.801(3)$, $\beta=102.818(3)$, $\gamma=$ 102.810(3), $V=1161.19(10)$ $10^6$ pm$^3$, $T=200$ K, $Z=2$, $\mu$(Mo-$K\alpha$) = 0.912 mm$^{-1}$, $D_{calcd.}=1.562$ g cm$^{-3}$; crystal dimensions $0.3\times0.2\times$ 0.05 mm$^3$, 15536 reflections, 6243 unique data, $R_{int}=0.0338$; 354 parameters, 0 restraints, $wR_2=0.1334$ (all data), $S=1.037$ (all data),

Research Article
doi.org/10.1002/ejic.202100898



$R_1 = 0.0466$ (5336 data with $I > 2\sigma(I)$), max/min residual electron density: $+0.70/-0.59$ e $10^{-6}$ pm$^{-3}$.

**3A**: $C_{27}H_{19}Cl_2F_3FeN_2Pd \cdot CH_2Cl_2$, 746.52 g mol$^{-1}$, monoclinic, $C2/c$, $a =$ 2840.91(18), $b = 2007.51(12)$, $c = 2319.20(13)$ pm, $\beta = 123.943(4)$, $V =$ 10972.8(12) $10^6$ pm$^3$, $T = 200$ K, $Z = 16$, $\mu$(Mo-$K\alpha$) = 1.617 mm$^{-1}$, $D_{calcd.} = 1.808$ g cm$^{-3}$; crystal dimensions $0.3 \times 0.1 \times 0.1$ mm$^3$, 24586 reflections, 10015 unique data, $R_{int} = 0.0444$; 759 parameters, 108 restraints, $wR_2 = 0.0972$, $S = 0.985$ (all data), $R_1 = 0.0383$ (6553 data with $I > 2\sigma(I)$), max/min residual electron density: $+0.37/-0.50$ e $10^{-6}$ pm$^{-3}$.

**4A**: $C_{54}H_{38}Cl_4Cu_2F_6Fe_2N_4 \cdot 3(C_7H_8)$, 1513.86 g mol$^{-1}$, triclinic, $P\bar{1}$, $a =$ 888.52(6), $b = 1284.61(9)$, $c = 1513.09(10)$ pm, $\alpha = 74.907(5)$, $\beta =$ 75.032(5), $\gamma = 78.908(5)$, $V = 1596.3(2)$ $10^6$ pm$^3$, $T = 200$ K, $Z = 1$, $\mu$(Mo-$K\alpha$) = 1.337 mm$^{-1}$, $D_{calcd.} = 1.575$ g cm$^{-3}$; crystal dimensions $0.5 \times 0.1 \times 0.05$ mm$^3$, 17431 reflections, 8565 unique data, $R_{int} =$ 0.0393; 460 parameters, 133 restraints, $wR_2 = 0.1024$, $S = 0.996$ (all data), $R_1 = 0.0364$ (6327 data with $I > 2\sigma(I)$), max/min residual electron density: $+0.47/-0.64$ e $10^{-6}$ pm$^{-3}$.

**5A**: $C_{36}H_{30}BrF_3FeN_2Ni$, 742.09 g mol$^{-1}$, triclinic, $P\bar{1}$, $a = 769.93(4)$, $b =$ 1027.90(6), $c = 2025.45(11)$ pm, $\alpha = 100.140(4)$, $\beta = 95.279(4)$, $\gamma =$ 107.753(4), $V = 1484.53(15)$ $10^6$ pm$^3$, $T = 200$ K, $Z = 2$, $\mu$(Mo-$K\alpha$) = 2.517 mm$^{-1}$, $D_{calcd.} = 1.660$ g cm$^{-3}$; crystal dimensions $0.3 \times 0.2 \times$ 0.02 mm$^3$, 12842 reflections, 6246 unique data, $R_{int} = 0.0570$; 431 parameters, 85 restraints, $wR_2 = 0.2239$, $S = 1.064$ (all data), $R_1 = 0.0705$ (4909 data with $I > 2\sigma(I)$), max/min residual electron density: $+1.06/-1.38$ e $10^{-6}$ pm$^{-3}$.

### Quantum chemical calculations

All density functional theory (DFT) calculations were performed with the program package TURBOMOLE applying different types of density functionals.[23] The vertical IPs were approximated on three different levels: (a) by Kohn-Sham orbital energies, (b) by ΔDFT, i.e. the difference of the DFT energies of the neutral ground state and ground state of the cation (structure of the neutral molecule), and (c) quasi-particle energies from eigenvalue only quasi-particle self-consistent GW (evGW) calculations.[24] The adiabatic ionization potential was obtained as in (b) but taking the energy of the optimized structure for the cation. With (b) only the first IP can be obtained while (a) and (c) allow to distinguish between ionization at Ni and Fe by a Mulliken population analysis of the ionized orbital. Reaction paths were obtained from calculations on model complexes where the Fe in the ferrocenyl unit was inactivated in a fixed oxidation state Fe(II) and Fe(III), respectively, by substituting it with a large core pseudopotential with the correct charge state (Figure 10). Transition states were preoptimized by a reaction path search from Plessow[25] and then determined by trust region image optimizations.[26] Within the here used model, the Fe(II) centre inside the ferrocenyl unit was replaced with the effective core potential ecp-28-mwb for Zn[27] and for modelling a Fe(III) centre with the effective core potential ecp-28-sdf for Ga[28] – both without basis sets and auxiliary basis sets to mimic the ionic character. A def2-TZVP basis set was used for the Ni atom, a def2-SV(P) basis was used for the rest of the ferrocenyl unit. A def2-SVP basis set was employed for all other atoms.[29,30] Dispersion corrections to DFT energies were taken into account using Grimme's D3 empirical method with Becke-Johnson damping (D3BJ).[31] The structures for the calculation of the IPs were searched and calculated with the B3LYP functional.[32] The energetic reaction pathways were explored with the BP86 functional.[33] All calculations were carried out in the gas phase.

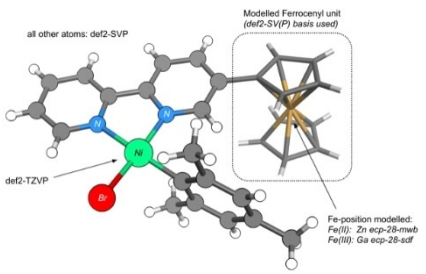


**Figure 10.** Overview about the employed catalyst model for **5D**. For further details, see the Supporting Information.

Deposition Numbers 2114838 (**1**), 2114839 (**2A**), 2114840 (**2C**), 2114841 (**3A**), 2114842 (**4A**), 2114843 (**5A**) contain the supplementary crystallographic data for this paper. These data are provided free of charge by the joint Cambridge Crystallographic Data Centre and Fachinformationszentrum Karlsruhe Access Structures service www.ccdc.cam.ac.uk/structures.

## Acknowledgements

*Financial support by the Collaborative Research Centre CRC/Transregio 88, "Cooperative effects in homo- and heterometallic complexes (3MET)" is gratefully acknowledged (Projects B4, B1, and A3). We thank Bernhard Birenheide for proof-reading the manuscript and Prof. Ignacio Fernández de las Nieves for his advice re NMR measurements. Open Access funding enabled and organized by Projekt DEAL.*

## Conflict of Interest

The authors declare no conflict of interest.

**Keywords:** Bimetallic complexes · Cooperative effects · Ferrocene · Metalloligands · Redox-switchable ligands

[1] Selected reviews: a) V. Blanco, D. A. Leigh, V. Marcos, *Chem. Soc. Rev.* **2015**, *44*, 5341–5370; b) J. Wei, P. L. Diaconescu, *Acc. Chem. Res.* **2019**, *52*, 415–424; c) O. R. Luca, C. H. Crabtree, *Chem. Soc. Rev.* **2013**, *42*, 1440–1459; d) A. M. Allgeier, C. A. Mirkin, *Angew. Chem. Int. Ed.* **1998**, *37*, 894–908; *Angew. Chem.* **1998**, *110*, 936–952; e) J. Choudhury, *Tetrahedron Lett.* **2018**, *59*, 487–558; f) E. V. Peris, M. Poyatos, S. Gonell, A. Gutiérrez-Blanco, C. Ruiz-Zambrana, *Angew. Chem. Int. Ed.* **2021**, *60*, 20003–20011; *Angew. Chem.* **2021**, *133*, 20156–20164.

[2] Selected reviews: a) R. Maiti, B. Birenheide, F. Breher, B. Sarkar, *ChemCatChem* **2021**, *13*, 2337–2370; b) Y. Ryu, G. Ahumada, C. W. Bielawski, *Chem. Commun.* **2019**, *55*, 4451–4466; c) E. Peris, *Chem. Rev.* **2018**, 118, 19, 9988–10031; d) A. Chirila, B. G. Das, P. F. Kuijpers, V. Sinha, B. de Bruin, *Non-Noble Metal Catalysis: Molecular Approaches and Reactions*, (Eds.: R. J. M. Klein Gebbink, M.-E. Moret), Wiley-VCH **2019**.

[3] I. M. Lorkovic, R. R. Duff, M. S. Wrighton, *J. Am. Chem. Soc.* **1995**, *117*, 3617–3618.

[4] Selected reviews on Fc-containing ligands: a) B. Bildstein, *J. Organomet. Chem.* **2001**, *617–618*, 28; b) U. Siemeling, *Eur. J. Inorg. Chem.* **2012**, 3523. Selected examples from the literature: c) E. M. Broderick, N. Guo, T. Wu, C. S. Vogel, C. Xu, J. Sutter, J. T. Miller, K. Meyer, T. Cantat, P. L. Diaconescu, *Chem. Commun.* **2011**, *47*, 9897–9899; d) E. M. Broderick, N. Guo, C. S. Vogel, C. Xu, J. Sutter, J. T. Miller, K. Meyer, P. Mehrkhodavandi, P. L. Diaconescu, *J. Am. Chem. Soc.* **2011**, *133*, 9278–9281; e) K. Arumugam, C. D. Varnado Jr, S. Sproules, V. M. Lynch, C. W. Bielawski, *Chem. Eur. J.* **2013**, *19*, 10866–10875; f) M. Süßner, H. Plenio, *Angew. Chem. Int. Ed.* **2005**, *44*, 6885–6888; *Angew. Chem.* **2005**, *117*, 7045–

7048; g) L. Hettmanczyk, S. Manck, C. Hoyer, S. Hohloch, B. Sarkar, *Chem. Commun.* **2015**, *51*, 10949–10952; h) L. Hettmanczyk, L. Suntrup, S. Klenk, C. Hoyer, B. Sarkar, *Chem. Eur. J.* **2017**, *23*, 576–585; i) S. Ibáñez, M. Poyatos, L. N. Dawe, D. Gusev, E. Peris, *Organometallics* **2016**, *35*, 2747–2758; j) P. Neumann, H. Dib, A.-M. Caminade, E. Hey-Hawkins, *Angew. Chem. Int. Ed.* **2015**, *54*, 311–314; *Angew. Chem.* **2015**, *127*, 316–319; k) M. Abubekerov, V. Vlček, J. Wei, M. E. Miehlich, S. M. Quan, K. Meyer, D. Neuhauser, P. L. Diaconescu, *iScience* **2018**, *7*, 120–131; l) M. Abubekerov, S. M. Shepard, P. L. Diaconescu, *Eur. J. Inorg. Chem.* **2016**, 2634–2640; m) A. B. Biernesser, K. R. Delle Chiaie, J. B. Curley, J. A. Byers, *Angew. Chem. Int. Ed.* **2016**, *55*, 5251–5254; *Angew. Chem.* **2016**, *128*, 5337–5340; n) C. K. A. Gregson, V. C. Gibson, N. J. Long, E. L. Marshall, P. J. Oxford, A. J. P. White, *J. Am. Chem. Soc.* **2006**, *128*, 7410–7411; o) J. M. Kaiser, B. K. Long, *Coord. Chem. Rev.* **2018**, *372*, 141–152; p) A. Lai, Z. C. Hern, P. L. Diaconescu, *ChemCatChem* **2019**, *11*, 4210–4218; q) M. Y. Lowe, S. Shu, S. M. Quan, P. L. Diaconescu, *Inorg. Chem. Front.* **2017**, *4*, 1798–1805; r) M. Qi, Q. Dong, D. Wang, J. A. Byers, *J. Am. Chem. Soc.* **2018**, *140*, 5686–5690.

[5] Contributions from our group: a) A. Feyrer, M. K. Armbruster, K. Fink, F. Breher, *Chem. Eur. J.* **2017**, *23*, 7402–7408; b) A. Feyrer, F. Breher, *Inorg. Chem. Front.* **2017**, *4*, 1125–1134; c) F. Walz, E. Moos, D. Garnier, R. Köppe, C. E. Anson, F. Breher, *Chem. Eur. J.* **2017**, *23*, 1173; d) E. Deck, H. E. Wagner, J. Paradies, F. Breher, *Chem. Commun.* **2019**, *55*, 5323–5326; e) S. Kaufmann, M. Radius, E. M. B. Moos, F. Breher, P. W. Roesky, *Organometallics* **2019**, *38*, 1721–1732; f) B. S. Birenheide, F. Krämer, L. Bayer, P. Mehlmann, F. Dielmann, F. Breher, *Chem. Eur. J.* **2021**, *27*, 15067–15074.

[6] a) D. Braga, M. Polito, M. Bracaccini, D. D'Addario, E. Tagliavini, D. M. Proserpio, F. Grepioni, *Chem. Commun.* **2002**, 1080–1081; b) D. Braga, M. Polito, M. Bracaccini, D. D'Addario, E. Tagliavini, L. Sturba, F. Grepioni, *Organometallics* **2003**, *22*, 2142–2150; c) D. Braga, D. D'Addari, M. Polito, F. Grepioni, *Organometallics* **2004**, *23*, 2810–2812; d) J. D. Crowley, I. M. Steele, B. Bosnich, *Chem. Eur. J.* **2006**, *12*, 8935–8951; e) S. Ø Scottwell, A. B. S. Elliott, K. J. Shaffer, A. Nafady, C. J. McAdam, K. C. Gordon, J. D. Crowley, *Chem. Commun.* **2015**, *51*, 8161–8164; f) J. A. Findlay, C. J. McAdam, J. J. Sutton, D. Preston, K. C. Gordon, J. D. Crowley, *Inorg. Chem.* **2018**, *57*, 3602–3614.

[7] a) D. H. Hua, J. W. McGill, M. Ueda, H. A. Stephany, *J. Organomet. Chem.* **2001**, *637–639*, 832–836; b) P. Beagley, M. A. L. Blackie, K. Chibale, C. Clarkson, R. Meijboom, J. R. Moss, P. J. Smith, H. Su, *Dalton Trans.* **2003**, 3046–3051; c) G. G. A. Balavoine, J. C. Daran, G. Iftime, E. Manoury, C. Moreau-Bossuet, *J. Organomet. Chem.* **1998**, *567*, 191–198; d) W. Hegazy, *Int. Res. J. Pure. Appl. Chem.* **2012**, *2*, 170–182; e) I. R. Butler, *Polyhedron* **1992**, *11*, 3117–3121; f) P. Štěpnička, T. Baše, *Inorg. Chem. Commun.* **2001**, *4*, 682–687; g) T.-Y. Dong, P.-J. Lin, K.-J. Lin, *Inorg. Chem.* **1996**, *35*, 6037–6044.

[8] R. M. G. Roberts, J. Silver, J. Azizian, *J. Organomet. Chem.* **1986**, *303*, 387–395.

[9] a) K. Nikitin, Y. Ortin, H. Müller-Bunz, D. G. Gilheany, M. J. McGlinchey, *Eur. J. Org. Chem.* **2018**, 5260–5267; b) N. Meyer, H. Schucht, C. W. Lehmann, B. Weibert, R. F. Winter, F. Mohr, *Eur. J. Inorg. Chem.* **2017**, 521–526; c) D. D. Swanson, K. M. Conner, S. N. Brown, *Dalton Trans.* **2017**, *46*, 9049–9057.

[10] a) R. Knapp, M. Rehahn, *J. Organomet. Chem.* **1993**, *452*, 235–240; b) K. Matsumoto, M. Suyama, S. Fujita, T. Moriwaki, Y. Sato, Y. Aso, S. Muroshita, H. Matsuo, K. Monda, K. Okuda, M. Abe, H. Fukunaga, A. Kano, M. Shindo, *Chem. Eur. J.* **2015**, *21*, 11590–11602; c) H. Braunschweig, B. Grünewald, K. Schwab, R. Sigritz, *Eur. J. Inorg. Chem.* **2009**, 4860–4863.

[11] B. Das, A. Kandegedara, L. Xu, T. Antonio, T. Stemmler, M. E. A. Reith, A. K. Dutta, *ACS Chem. Neurosci.* **2017**, *8*, 723–730.

[12] S. Ø Scottwell, K. J. Shaffer, C. J. McAdam, J. D. Crowley, *RSC Adv.* **2014**, *4*, 35726–35734.

[13] K. Molčanov, V. Milašinović, B. Kojić-Prodić, *Cryst. Growth Des.* **2019**, *19*, 5967–5980.

[14] a) V. E. Albrow, A. J. Blake, R. Fryatt, C. Wilson, S. Woodward, *Eur. J. Org. Chem.* **2006**, 2549–2557; b) C. J. McAdam, B. H. Robinson, J. Simpson, *Acta Crystallogr. Sect. E* **2003**, *59*, m687–m689; c) O. Kadkin, C. Näther, W. Friedrichsen, *J. Organomet. Chem.* **2002**, *649*, 161–172.

[15] a) M. a Hernández-Molina, J. González-Platas, C. Ruiz-Pérez, F. Lloret, M. Julve, *Inorg. Chim. Acta* **1999**, *284*, 258–265; b) A. M. Prokhorov, P. A. Slepukhin, D. N. Kozhevnikov, *J. Organomet. Chem.* **2008**, *693*, 1886–1894; c) E. Tynan, P. Jensen, A. C. Lees, B. Moubaraki, K. S. Murray, P. E. Kruger, *CrystEngComm* **2005**, *7*, 90–95; d) M. D. Stephenson, M. J. Hardie, *Dalton Trans.* **2006**, 3407–3417; e) E. Kövári, R. Krämer, *Z. Naturforsch. B* **1994**, *49*, 1324–1328; f) E. Liu, Y. Z. Zhang, L. Li, C. Yang, J. C. Fettinger, G. Zhang, *Polyhedron* **2015**, *99*, 223–229; g) C. E. Sutton, L. P. Harding, M. Hardie, T. Riis-Johannessen, C. R. Rice, *Chem. Eur. J.* **2012**, *18*, 3464–3467; h) M. T. Garland, D. Grandjean, E. Spodine, A. M. Atria, J. Manzur, *Acta Crystallogr. Sect. C* **1988**, *44*, 1209–1212; i) O. Gonzalez Q, A. M. Atria, E. Spodine, J. Manzur, M. T. Garland, *Acta Crystallogr. Sect. C* **1993**, *49*, 1589–1591.

[16] A. Klein, *Z. Anorg. Allg. Chem.* **2001**, *627*, 645–650.

[17] a) D. M. Khramov, E. L. Rosen, V. M. Lynch, C. W. Bielawski, *Angew. Chem. Int. Ed.* **2008**, *47*, 2267–2270; *Angew. Chem.* **2008**, *120*, 2299–2302; b) B. L. Blass, R. Hernández Sánchez, V. A. Decker, M. J. Robinson, N. A. Piro, W. S. Kassel, P. L. Diaconescu, C. Nataro, *Organometallics* **2016**, *35*, 462–470; c) K. Jess, D. Baabe, T. Bannenberg, K. Brandhorst, M. Freytag, P. G. Jones, M. Tamm, *Inorg. Chem.* **2015**, *54*, 12032–12045.

[18] a) C. Elschenbroich, M. Cais, *J. Organomet. Chem.* **1969**, *18*, 135–143; b) J. Carbajo, S. Bollo, L. J. Núñez-Vergara, A. Campero, J. A. Squella, *J. Electroanal. Chem.* **2002**, *531*, 187–194; c) D. Basu, S. Mazumder, K. K. Kpogo, C. N. Verani, *Dalton Trans.* **2019**, *48*, 14669–14677.

[19] a) A. Klein, A. Kaiser, W. Wielandt, F. Belaj, E. Wendel, H. Bertagnolli, S. Záliš, *Inorg. Chem.* **2008**, *47*, 11324–11333; b) J. A. Terrett, J. D. Cuthbertson, V. W. Shurtleff, D. W. MacMillan, *Nature* **2015**, *524*, 330–334.

[20] J. B. Diccianni, T. Diao, *Trends Chem.* **2019**, *1*, 830–844.

[21] T. Hayashida, H. Kondo, J.-i. Terasawa, K. Kirchner, Y. Sunada, H. Nagashima, *J. Organomet. Chem.* **2007**, *692*, 382–394.

[22] a) G. M. Sheldrick, *Acta Crystallogr. Sect. A* **2015**, *A71*, 3–8; b) G. M. Sheldrick, *Acta Crystallogr. Sect. C* **2015**, *C71*, 3–8.

[23] S. G. Balasubramani, G. P. Chen, S. Coriani, M. Diedenhofen, M. S. Frank, Y. J. Franzke, F. Furche, R. Grotjahn, M. E. Harding, C. Hättig, A. Hellweg, B. Helmich-Paris, C. Holzer, U. Huniar, M. Kaupp, A. M. Khah, S. K. Khani, T. Müller, F. Mack, B. D. Nguyen, S. M. Parker, E. Perlt, D. Rappoport, K. Reiter, S. Roy, M. Rückert, G. Schmitz, M. Sierka, E. Tapavicza, D. P. Tew, C. van Wüllen, V. K. Voora, F. Weigend, A. Wodyński, J. M. Yu, *J. Chem. Phys.* **2020**, *152*, 184107.

[24] M. J. van Setten, F. Weigend, F. Evers, *J. Chem. Theory Comput.* **2013**, *9*, 232–246.

[25] P. Plessow, *J. Chem. Theory Comput.* **2013**, *9*, 1305–1310.

[26] T. Helgaker, *Chem. Phys. Lett.* **1991**, *182*, 503–510.

[27] F. Schautz, H.-J. Flad, M. Dolg, *Theor. Chem. Acc.* **1998**, *99*, 231–240.

[28] G. Igel-Mann, H. Stoll, H. Preuss, *Mol. Phys.* **1988**, *65*, 1321–1328.

[29] A. Schäfer, H. Horn, R. Ahlrichs, *J. Chem. Phys.* **1992**, *97*, 2571–2577.

[30] A. Schäfer, C. Huber, R. Ahlrichs, *J. Chem. Phys.* **1994**, *100*, 5829–5835.

[31] a) S. Grimme, J. Antony, S. Ehrlich, H. Krieg, *J. Chem. Phys.* **2010**, *132*, 154104; b) S. Grimme, S. Ehrlich, L. Goerigk, *J. Comput. Chem.* **2011**, *32*, 1456–1465.

[32] A. D. Becke, *J. Chem. Phys.* **1993**, *98*, 5648–5652.

[33] A. D. Becke, *Phys. Rev. A* **1988**, *38*, 3098–3100.

Manuscript received: October 18, 2021
Revised manuscript received: December 13, 2021
Accepted manuscript online: December 13, 2021

## RESEARCH ARTICLE

**FcBipy**: Novel redox-active bipyridine ligands based on 1,1′ difunctionalized ferrocenyl backbone, in conjunction with their metal complexes, are reported. The influence of the implemented functional groups on both the iron-centred redox potential and the *N*,*N*′-coordinated nickel complexes were confirmed for the reductive elimination reaction of an aryl ether induced by oxidation of the corresponding methoxides.

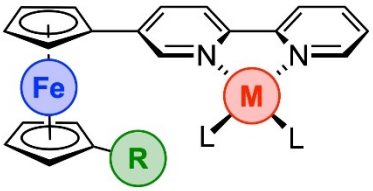


Influence of **R** on $E^0_{1/2}$(**Fe**) and reactivity of **M** ???

*Dr. H. E. Wagner, N. Frank, E. Barani, Dr. C. E. Anson, L. Bayer, Prof. Dr. A. K. Powell, Prof. Dr. K. Fink, Prof. Dr. F. Breher**